Angewandte Chemie
Eine Zeitschrift der Gesellschaft Deutscher Chemiker

Supporting Information

Loading Linear Arrays of Cu^{II} Inside Aromatic Amide Helices

*Jinhua Wang, Barbara Wicher, Alejandro Méndez-Ardoy, Xuesong Li, Gilles Pecastaings, Thierry Buffeteau, Dario M. Bassani, Victor Maurizot, and Ivan Huc**

anie_202104734_sm_miscellaneous_information.pdf

Contents:

General Remarks: All the solvents and reagents were used as received from commercial sources unless otherwise specified. Dry dichloromethane (DCM, CH_2Cl_2) was obtained from a solvent drying system passing through alumina columns; chloroform ($CHCl_3$) and diisopropylethylamine (DIEA) were distilled over calcium hydride (CaH_2) prior to use. Reactions were monitored by thin layer chromatography (TLC) on Merck silica gel 60-F254 plates and observed under UV light. Silica gel column chromatography purifications were carried out on Merck GEDURAN Si60 (40-63 µm). Preparative recycling Gel Permeation Chromatography (GPC) was performed on a JAI LC-9130G NEXT using two JAIGEL 20×600 mm columns (Japan Analytical Industry) with 0.5 % NEt_3 and 1% ethanol in chloroform (HPLC grade, ethanol stabilized), as mobile phase, with a flow rate of 7 mL/min. ^{1}H NMR spectra were recorded on BRUKER AVANCE 300 MHz or 400 MHz spectrometers. Chemical shifts were presented in parts per million (δ, ppm) using solvent residue peaks as references (chloroform δ = 7.26 ppm). Coupling constants are reported as Hertz. ESI mass spectra were measured in the Mass Spectrometry Laboratory at the European Institute of Chemistry and Biology (UMS 3033 - IECB), Pessac, France. UV-Vis spectroscopy was recorded on Varian® Cary 300 Scan UV-Visible spectrophotometer at room temperature. FTIR spectroscopy was recorded on Bruker IRFT IFS 55 infrared spectrometer using KBr to make the pallet and the spectrum was recorded at room temperature.

1. Oligomer synthesis:

1.1 Q_n oligomers synthesis

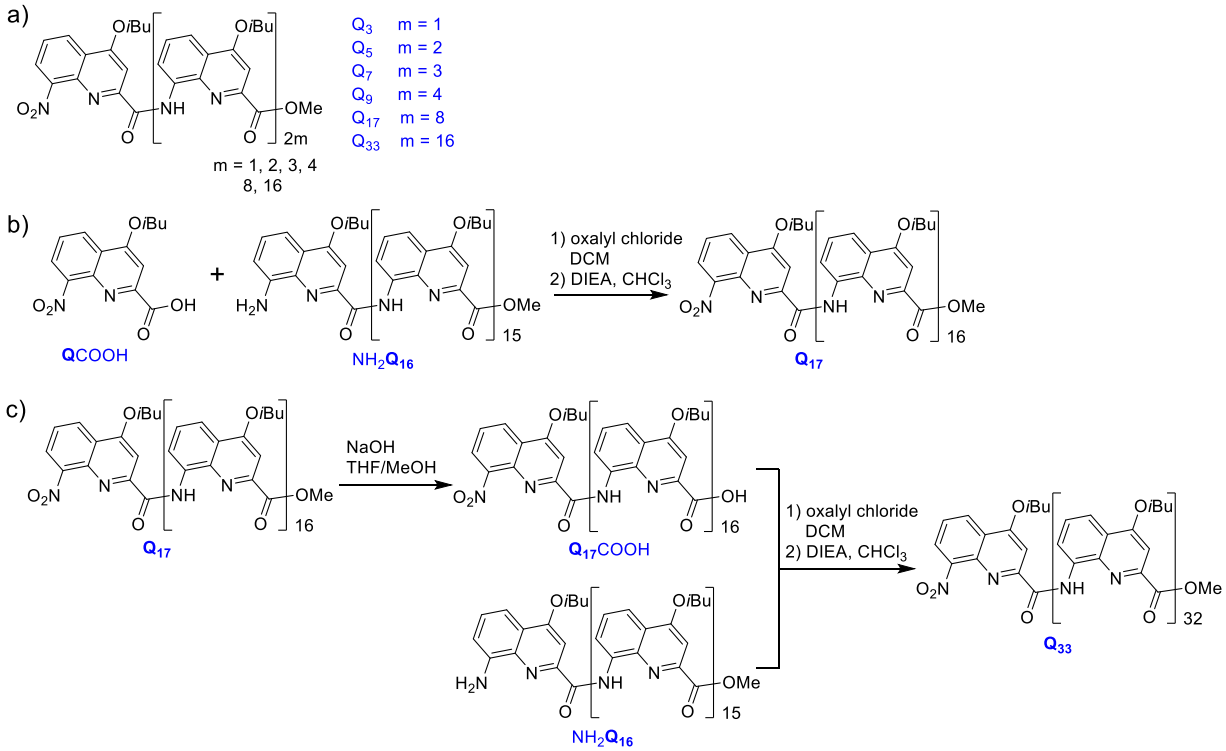

Scheme S1: a) Chemical structures of quinoline oligoamide foldamers with odd numbers of quinoline units (3 to 33 units); the synthetic routes for b) Q_{17} and c) Q_{33}.

Quinolinecarboxamide oligomers from Q_3 to Q_9 have been reported previously[1] and were prepared according to previous established methods with minor changes.[1-2] The longer oligomers Q_{17} and Q_{33} were prepared by segment coupling methods according to the scheme showed in Figure S1 and were purified with GPC.[3] Intermediates QCOOH[2], NH_2Q_{16}[3a] have been reported previously.

Q_{17}: QCOOH was activated with oxalyl chloride according to a known procedure.[2] QCOOH was dissolved in dry chloroform and mixed with oxalyl chloride. After stirring at room temperature for 2 h, the acid was completely converted to the corresponding acid chloride as indicated by the crude ^{1}H NMR. Solvent and excess oxalyl chloride were removed under high vacuum for at least 3 h without any other treatments. The acid chloride of QCOOH (QCOCl, 1.5 equiv. with respect to NH_2Q_{16}) was dissolved in a minimum amount of dry chloroform and transferred into a flask containing NH_2Q_{16} (230 mg, 0.058 mmol). Dry DIEA (2 equiv. with respect to NH_2Q_{16}) was added into the mixture. The reaction was then kept at room temperature under N_2 overnight. Solvents were removed and the residue was redissolved in $CHCl_3$ and purified by GPC. Yield: 210 mg (85%). ^{1}H NMR (300 MHz, $CDCl_3$): δ 11.11 (s, 1 H), 11.05 (s, 1 H), 10.68 (s, 1 H), 10.67 (s, 1 H), 10.48 (s, 1 H), 10.32 (s, 1 H), 10.28 (s, 1 H), 10.18 (s, 1 H), 10.12 (s, 1 H), 10.05 (s, 1 H), 10.03 (s, 1 H), 9.98 (s, 2 H), 9.93 (s, 1 H), 9.91 (s, 2 H), 8.16 (dd, *J* = 7.9, 1.5 Hz, 1 H), 7.94 (d, *J* = 7.3 Hz, 1 H), 7.87 (dd, *J* = 7.8, 3.7 Hz, 1 H), 7.86 (dd, *J* = 7.8, 3.7 Hz, 1 H), 7.80 – 7.76 (m, 4 H), 7.73 (d, *J* = 8.4 Hz, 1 H), 7.67 – 7.53 (m, 12 H), 7.23 (s, 1 H), 7.20 (s, 2 H), 7.19 – 7.08 (m, 5 H), 7.08 – 6.71 (m, 23 H), 6.41 (s, 1 H), 6.38 (s, 1 H), 6.21 (s, 1 H), 6.16 (s, 1 H), 6.13 (s, 1 H), 5.90 (s, 1 H), 5.86 (s, 1 H), 5.85 (s, 1 H), 5.78 – 5.68 (m, 7 H), 3.91 (m, 4 H), 3.81 – 3.62 (m, 20 H), 3.59 – 3.45 (m, 11 H), 2.83 (s, 3 H), 2.36 – 2.06 (m, 17 H), 1.30 – 0.95 (m, 120 H) ppm; HRMS (ESI+) m/z: calcd for $C_{239}H_{242}N_{34}O_{37}$ $[M+2H]^{2+}$ 2090.9084, found 2090.9022.

Q_{17}COOH: This compound was prepared according a previously reported procedure[3a]. Q_{17} (110 mg, 0.026) and sodium hydroxide (21 mg, 0.53 mmol) were dissolved in 2 mL of THF/MeOH (vol/vol 9:1) and stirred at room temperature for 2 hours. After complete consumption of the starting Q_{17} (indicated by TLC), water was added followed by a 5% aqueous citric acid solution to adjust the pH to ~5. Dichloromethane was added and the organic layer was collected. The solvent was dried over Na_2SO_4, filtered, and evaporated. The residual solid was dissolved in a minimum amount of $CHCl_3$ and precipitated by addition of methanol. The solid was collected and dried under high vacuum. Yield: (100 mg, 92%). ^{1}H NMR (300 MHz, $CDCl_3$): δ 10.88 (s, 1 H), 10.68 (s, 1 H), 10.67 (s, 1 H), 10.51 (s, 1 H), 10.48 (s, 1 H), 10.32 (s, 1 H), 10.31 (s, 1 H), 10.18 (s, 1 H), 10.16 (s, 1 H), 10.05 (s, 2 H), 9.98 (s, 2 H), 9.93 (s, 1 H), 9.91 (s, 2 H), 8.17 (d, *J* = 6.9 Hz, 1 H), 8.03 – 7.93 (m, 3 H), 7.86 (d, *J* = 7.4 Hz, 1 H), 7.81 – 7.75 (m, 6 H), 7.72 – 7.69 (m, 2 H), 7.69 – 7.56 (m, 14 H), 7.22 (d, *J* = 4.8 Hz, 2 H), 7.18 – 7.08 (m, 4 H), 7.07 – 6.90 (m, 14 H), 6.88 (s, 1 H), 6.85 (s, 1 H), 6.84 – 6.73 (m, 9 H), 6.54 (s, 1 H), 6.45 (s, 1 H), 6.32 (s, 1 H), 6.10 (s, 1 H), 6.09 (s, 1 H), 5.90 (s, 1 H), 5.86 (s, 1 H), 5.85 (s, 1 H), 5.78 (s, 1 H), 5.76 (s, 1 H), 5.75 (s, 1 H), 5.74 (s, 1 H), 5.72 (s, 1 H), 5.70 (s, 1 H), 5.69 (s, 1 H), 3.97 – 3.44 (m, 45 H), 2.44 – 2.18 (m, 27 H), 1.26 – 1.01 (m, 120 H) ppm.

Q_{33}: This compound was prepared by segment couplings as showed in Figure S1. Q_{17}COOH was activated to the corresponding acid chloride (Q_{17}COCl) by using oxalyl chloride according to an earlier report.[3a] Q_{17}COCl (2 equiv. with respect to NH_2Q_{16}) was dissolved in minimum amount of dry $CHCl_3$ and transferred to a flask containing NH_2Q_{16} (200 mg, 0.048 mmol). Dry DIEA (3 equiv. with respect to NH_2Q_{16}) was added, and the reaction mixture was kept at room temperature overnight. Then the solvent was removed and 3 mL of pyridine and 3 drops of H_2O were added to the solid residue. The solution was heated at 80 °C for 6 hours. After cooling to room temperature, the mixture was diluted with DCM and washed with water and an aqueous citric acid solution (5%). The organic layer was collected, dried over Na_2SO_4, filtered and the solvent was removed under reduced pressure. The residue was dissolved in $CHCl_3$ and purified with GPC. Yield: 240 mg (60%). ^{1}H NMR (300 MHz, $CDCl_3$): δ 11.03 (s, 1 H), 11.00 (s, 1 H), 10.62 (s, 1 H), 10.60 (s, 1 H), 10.40 (s, 1 H), 10.23 (s, 1 H), 10.18 (s, 1 H),

10.07 (s, 1 H), 10.01 (s, 1 H), 9.91 (s, 1 H), 9.89 (s, 1 H), 9.81 (s, 2 H), 9.70 (s, 1 H), 9.69 (s, 1 H), 9.63 (s, 2 H), 9.57 – 9.45 (m, 15 H), 8.11 (d, *J* = 8.0 Hz, 1 H), 7.88 (d, *J* = 7.5 Hz, 1 H), 7.81 (t, *J* = 7.2 Hz, 2 H), 7.73 – 7.26 (m, 45 H), 7.18 – 6.46 (m, 71 H), 6.34 (s, 1 H), 6.32 (s, 1 H), 6.16 (s, 1 H), 6.08 (s, 1 H), 6.04 (s, 1 H), 5.81 (s, 1 H), 5.78 (s, 1 H), 5.75 (s, 1 H), 5.65 (s, 1 H), 5.63 (s, 1 H), 5.61 (s, 1 H), 5.60 (s, 1 H), 5.57 (s, 1 H), 5.51 – 5.39 (m, 20 H), 5.30 (s, 2 H), 3.95 – 3.17 (m, 74 H), 2.78 (s, 3 H), 2.31 – 1.98 (m, 40 H), 1.16 – 0.94 (m, 240 H) ppm; HRMS (ESI+) m/z: calcd for $C_{463}H_{468}N_{66}O_{69}$ $[M+4H]^{4+}$ 2015.1327, found 2015.1288.

1.2 $AsgQ_n$ oligomers synthesis

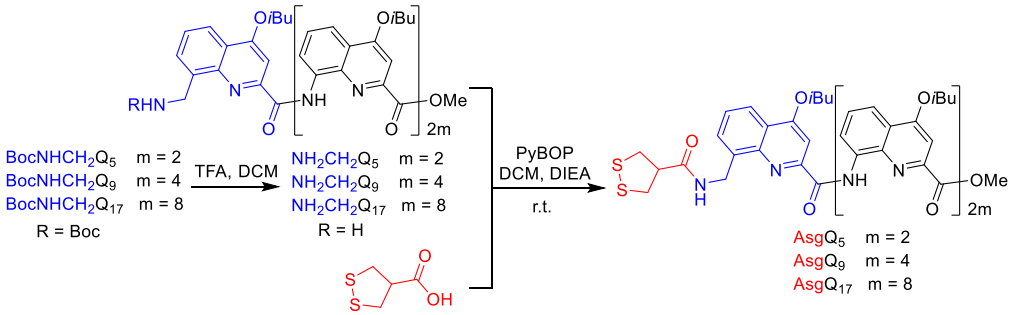

Scheme S2: Synthesis of the asparagusic functionalized quinoline oligoamide foldamers.

Shorter $BocNHCH_2Q_n$ (n = 5, 9, 17) oligomers have been reported previously and were synthesized according to reported procedures.[4] Asparagusic acid was prepared according to literature procedures.[5]

General procedure for coupling of the asparagusic unit to oligomers: The corresponding Boc-protected $BocNHCH_2Q_n$ (n = 5, 9, 17) oligomer was first treated with TFA to remove the Boc-protecting group. The starting material (100 mg) was dissolved in 3 mL of dry dichloromethane. Then 1 mL of TFA was added and the mixture was stirred at room temperature for 2 hours. After that, the reaction mixture was diluted with dichloromethane (10 mL) and washed one time with water and three times with a $NaHCO_3$ aqueous solution (10%) to completely remove TFA. The organic layer was dried over Na_2SO_4, filtered and solvents were evaporated. The solid was dried under high vacuum and was used for the coupling reaction directly without further purification. This free amine was mixed with asparagusic acid (1.5 equiv. with respect to the amine), pyBOP (5 equiv.), and dry DIEA (2 equiv.) in dry chloroform (2 mL) under anhydrous conditions. The resulting mixture was stirred at room temperature under N_2 overnight. Then, the solvent was removed and the product was purified by GPC directly without other treatments. The clean fraction of the product was collected and solvents were removed. The solid was dried under high vacuum to yield a slight yellow solid.

$AsgQ_5$: Starting with 250 mg of $BocNHCH_2Q_5$, Yield: 235 mg (92%). ^{1}H NMR (300 MHz, $CDCl_3$): δ 11.93 (s, 1 H), 11.81 (s, 1 H), 11.79 (s, 1 H), 11.53 (s, 1 H), 8.54 (dt, *J* = 7.7, 1.5 Hz, 2 H), 8.21 (dd, *J* = 8.4, 1.4 Hz, 1 H), 8.18 – 8.05 (m, 3 H), 8.03 – 7.96 (m, 2 H), 7.89 (dd, *J* = 8.5, 1.4 Hz, 1 H), 7.70 – 7.43 (m, 2 H), 7.42 (s, 1 H), 7.37 (t, *J* = 8.0 Hz, 1 H), 7.31 (d, *J* = 7.9 Hz, 1 H), 7.21 (t, *J* = 6.9 Hz, 1 H), 6.82 (s, 1 H), 6.77 (s, 1 H), 6.70 (d, *J* = 6.9 Hz, 1 H), 6.58 (s, 1 H), 5.09 (br, 1 H), 4.42 (dd, *J* = 9.0, 6.2 Hz, 1 H), 4.37 – 4.27 (m, 1 H), 4.22 (dd, *J* = 9.0, 6.9 Hz, 1 H), 4.15 (d, *J* = 5.8 Hz, 1 H), 4.09 (t, *J* = 6.8 Hz, 1 H), 4.01 – 3.90 (m, 3 H), 3.90 – 3.83 (m, 1 H), 3.80 (d, *J* = 6.3 Hz, 2 H), 3.59 (dd, *J* = 15.4, 6.9 Hz, 1 H), 3.19 (s, 3 H), 2.61 – 2.21 (m, 5 H), 1.38 – 1.14 (m, 44 H) ppm; HRMS (ESI+) m/z: calcd for $C_{76}H_{81}N_{10}O_{12}S_2$ $[M+H]^+$ 1389.5477, found 1389.5507.

AsgQ$_9$: Starting with 100 mg BocNHCH$_2$Q$_9$, Yield: 88 mg (87%). ^{1}H NMR (300 MHz, $CDCl_3$): δ 11.44 (s, 1 H), 11.30 (s, 1 H), 11.14 (s, 1 H), 10.95 (s, 1 H), 10.90 (s, 1 H), 10.83 (s, 1 H), 10.78 (s, 1 H), 10.71 (s, 1 H), 8.17 (d, *J* = 7.6 Hz, 1 H), 8.16 (d, *J* = 7.4 Hz, 1 H), 8.11 (d, *J* = 8.4 Hz, 2 H), 8.06 – 7.99 (m, 2 H), 7.95 – 7.87 (m, 3 H), 7.83 (dd, *J* = 8.3, 1.2 Hz, 1 H), 7.80 – 7.72 (m, 4 H), 7.71 (dd, *J* = 8.3, 1.2 Hz, 1 H), 7.67 – 7.60 (m, 3 H), 7.57 – 7.51 (m, 3 H), 7.43 – 7.28 (m, 6 H), 7.22 (t, *J* = 7.6 Hz, 2 H), 7.14 (t, *J* = 7.9 Hz, 1 H), 7.05 (t, *J* = 7.9 Hz, 1 H), 6.99 (dd, *J* = 8.6, 6.9 Hz, 2 H), 6.92 (s, 1 H), 6.85 (s, 1 H), 6.66 (s, 1 H), 6.53 (s, 1 H), 6.49 (s, 1 H), 6.41 (d, *J* = 8.4 Hz, 1 H), 6.40 (s, 1 H), 6.35 (s, 1 H), 6.17 (s, 1 H), 6.05 (s, 1 H), 4.40 (br, 1 H), 4.17 – 3.56 (m, 23 H), 3.31 – 3.15 (m, 3 H), 2.99 (s, 3 H), 2.84 (dd, *J* = 11.4, 7.4 Hz, 1 H), 2.78 – 2.68 (m, 3 H), 2.54 – 2.15 (m, 10 H), 1.38 – 1.09 (m, 74 H) ppm; HRMS (ESI+) m/z: calcd for $C_{132}H_{137}N_{18}O_{20}S_2$ $[M+H]^+$ 2358.9732, found 2358.9730.

AsgQ$_{17}$: Starting with 55 mg BocNHCH$_2$Q$_{17}$, Yield 50 mg (91%). ^{1}H NMR (300 MHz, $CDCl_3$): δ 11.11 (s, 1 H), 11.05 (s, 1 H), 10.73 (s, 1 H), 10.66 (s, 1 H), 10.49 (s, 1 H), 10.28 (s, 1 H), 10.25 (s, 1 H), 10.18 (s, 1H), 10.13 (s, 1 H), 10.08 (s, 1 H), 10.04 (s, 1 H), 9.99 (s, 2 H), 9.95 (s, 1 H), 9.92 (s, 1 H), 9.91 (s, 1 H), 7.94 (d, *J* = 7.4 Hz, 1 H), 7.87 (d, *J* = 7.3 Hz, 1 H), 7.83 (d, *J* = 7.5 Hz, 1 H), 7.79 (m, 3 H), 7.75 – 7.52 (m, 13 H), 7.24 (d, *J* = 7.6 Hz, 1 H), 7.20 (t, *J* = 7.7 Hz, 1 H), 7.15 – 7.08 (m, 3 H), 7.05 – 6.91 (m, 10 H), 6.90 – 6.74 (m, 10 H), 6.72 (s, 1 H), 6.69 (s, 1 H), 6.41 (s, 1 H), 6.37 (s, 1 H), 6.26 (d, *J* = 6.8 Hz, 1 H), 6.21 (s, 1 H), 6.15 (s, 1 H), 6.13 (s, 1 H), 5.89 (s, 1 H), 5.86 (s, 1 H), 5.80 (s, 1 H), 5.76 (s, 2 H), 5.75 (s, 1 H), 5.73 (s, 1 H), 5.71 (s, 1 H), 5.70 (s, 2 H), 4.18 (br, 1 H), 3.96 – 3.85 (m, 4 H), 3.82 – 3.39 (m, 34 H), 3.05 – 2.96 (m, 1 H), 2.82 (s, 3 H), 2.73 (dd, *J* = 11.3, 7.4 Hz, 1 H), 2.66 – 2.58 (m, 2 H), 2.40 – 2.04 (m, 20 H), 1.29 – 0.93 (m, 116 H) ppm; HRMS (ESI+) m/z: calcd for $C_{244}H_{250}N_{34}O_{36}S_2$ $[M+2H]^{2+}$ 2148.9143, found 2148.9172.

2. Complexation with metals:

2.1 Metal complexation with Q_n (n = 3, 5, 7, 9, 17, 33) oligomers

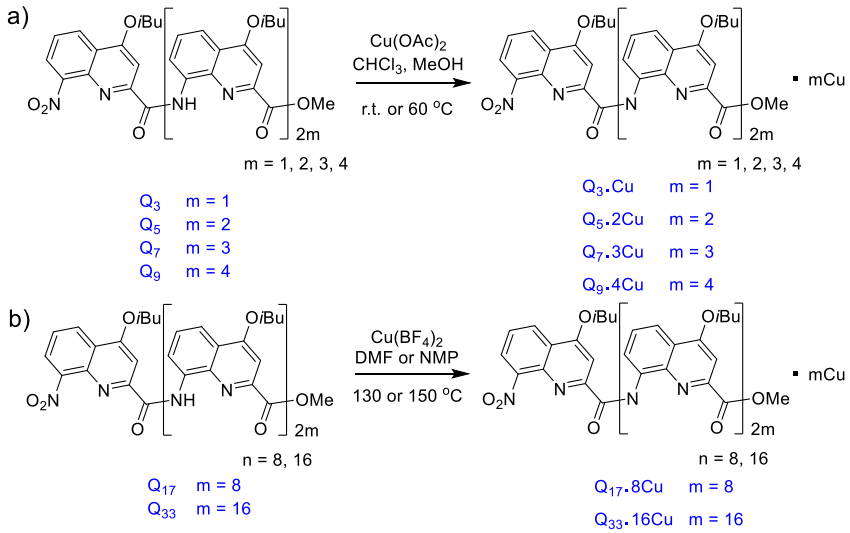

Scheme S3: Reactions for the loading Copper (II) ions inside the quinoline carboxamide oligomers of length a) 3, 5, 7, and 9 units and b) 17 and 33 units.

For metal ions like Zn (II) and Pd (II) that are diamagnetic, NMR was used as tool to follow the reaction. Typically, 0.5 mmol of the quinolinecarboxamide oligomer and 1 equiv. of the metal salts per coordination site were introduced into an NMR tube. Then 0.5 mL of solvents, typically $CDCl_3$ or a mixture of $CDCl_3$ and MeOD-D_4 depending on the solubility, were added. Then NMR spectra were recorded after waiting certain period of time either at room temperature or at elevated temperature depending on the reaction kinetics.

For Cu(II) metal ions where NMR was not suitable due to the paramagnetic nature of the Cu(II) ion, the reaction was followed by UV-Vis spectra where significant differences of absorption were observed as well as by MS. Typically, 15 mg of the quinolinecarboxamide oligomer (from Q_3 to Q_9) were added into a flask and dissolved in around 2-3 mL of chloroform. Then 2-3 equivalents of $Cu(OAc)_2$ per coordination site of the oligomers were dissolved in a minimum amount of methanol and added into the quinolinecarboxamide solution. The resulting mixture was stirred either at room temperature (for Q_3 and Q_5) or at 65 ^oC (for Q_7 to Q_9). After completion (as confirmed by both UV-Vis and MS measurements) the reaction was diluted with dichloromethane and washed with water to remove excess salts. The organic layer was separated and the solvent was evaporated to result a dark green solid. For longer oligomers, like Q_{17} and Q_{33}, the reaction was carried out in dry DMF (for Q_{17}) or dry NMP (for Q_{33}). For both oligomers, the copper salt used was copper tetrafluoroborate which was dried under high vacuum prior usage.

Q_{17}•8Cu: 15 mg of Q_{17} and about 30 mg of $Cu(BF_4)_2$ were dissolved in 3 mL of dry DMF under inert atmosphere. The mixture was heated at 120 ^oC for 15 minutes and cooled down to room temperature. Dichloromethane was added and the organic layer was washed with water and evaporated to yield a dark solid.

Q_{33}•16Cu, the reaction conditions were similar to Q_{17}•8Cu except the solvent changed to NMP and heated at 150 ^oC for about 20 minutes before cooling down.

2.2 Calculation of the number of intermediates:

Definition: $C_n^k = \frac{n!}{k!\cdot(n-k)!}$ $(k \leq n)$

Note: Combination numbers were calculated by using the COMBIN function of MS Excel software.

For Q_{2n+1}•nCu oligomers, intermediates may contain 1, 2…and (n-1) Cu, hence the total number of intermediates is the sum of all those intermediates containing 1, 2…and (n-1) Cu. For an intermediate that contains k Cu ($k \leq n-1$), the number of different Cu arrangements is: C_{2n-k}^k, hence, the total number of intermediates is: $C_{2n-1}^1 + C_{2n-2}^2 + \cdots + C_{n+1}^{n-1}$.

The productive intermediates are those where each Cu is a position conducive to full loading without error correction. It thus the sum all productive intermediates containing 1, 2…and up to (n-1) Cu. For productive intermediates that contain k Cu ($k \leq n-1$), the number of possibilities is: C_n^k, hence, the total number of productive intermediates is: $C_n^1 + C_n^2 + \cdots + C_n^{n-1}$.

The saturated intermediates are those do not have consecutive empty sites. For Q_9•4Cu, at least 3 Cu are required in order not to leave two consecutive empty sites. After taking up 3 Cu, there are 2 empty sites left in Q_9. The 3 Cu defines 4 locations (possible orphan NH sites in between them and at the ends) where to distribute the two empty sites, *i.e.* C_4^2 combinations. For Q_{33}•16Cu, at least 11 Cu are required. These 11 Cu define 12 locations to distribute 10 empty sites, *i.e.* C_{12}^{10} combinations. When 12, 13, 14, 15 Cu are taken up, they define 13, 14, 15, 16 locations, respectively, where to distribute 8, 6, 4, and 2 empty sites, respectively.

For Q_9•4Cu:
The number of possible intermediates is: $C_7^1 + C_6^2 + C_5^3 = 32$.
The number of productive intermediates is: $C_4^1 + C_4^2 + C_4^3 = 14$.
The number of saturated intermediates is: $C_4^2 = 6$.

For Q_{33}•16Cu:
The number of possible intermediates is: $C_{31}^1 + C_{30}^2 + C_{29}^3 + C_{28}^4 + C_{27}^5 + C_{26}^6 + C_{25}^7 + C_{24}^8 +$

$C_{23}^{9} + C_{22}^{10} + C_{21}^{11} + C_{20}^{12} + C_{19}^{13} + C_{18}^{14} + C_{17}^{15} = 3524576 \approx 3.5 \times 10^{6}$.

The number of productive intermediates is: $C_{16}^{1} + C_{16}^{2} + C_{16}^{3} + C_{16}^{4} + C_{16}^{5} + C_{16}^{6} + C_{16}^{7} + C_{16}^{8} + C_{16}^{9} + C_{16}^{10} + C_{16}^{11} + C_{16}^{12} + C_{16}^{13} + C_{16}^{14} + C_{16}^{15} = 65534 \approx 6.5 \times 10^{4}$.

The number of saturated intermediates is: $C_{12}^{10} + C_{13}^{8} + C_{14}^{6} + C_{15}^{4} + C_{16}^{2} = 5841$.

2.3 Cu(II) loading of $AsgQ_n$ (n = 5, 9, 17) oligomers:

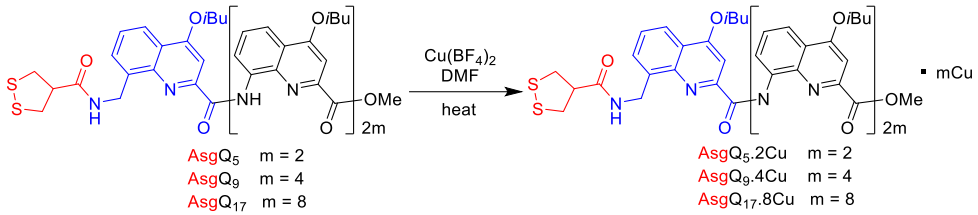

Scheme S4: Reaction scheme of the loading of Cu(II) into the $AsgQ_n$ (n = 5, 9, 17) oligomers.

The asparagusic group at the extremity of $AsgQ_n$ (n = 5, 9, 17) oligomers serves as an anchoring group for the formation of self-assembled monolayers on the surface of gold. The asparagusic group was chosen because of the relative stability of the disulfide group which may allow us to bypass any problem of coordination of copper to thiols which are also commonly used to prepare SAM on gold nanoparticles and gold surfaces. The complexation with copper was based on the above mentioned methods to load copper into the Q_n oligomers. In order to avoid as much as possible decomposition or any side reactions associated with the asparagusic group (for example the disulfide bond), the reaction time was carefully optimized by monitoring the reactions with ESI-MS. The loading of Cu(II) into all three $AsgQ_n$ (n = 5, 9, 17) oligomers were performed in dry DMF using $Cu(BF_4)_2$ as copper salt. The reaction temperatures were different depending on the oligomers length. For $AsgQ_5$, the reaction was performed at 80 °C, for $AsgQ_9$, the reaction was performed at 140 °C and for $AsgQ_{17}$ the reaction was performed at 155 °C. The formation of the desired clean products was confirmed by ESI+ MS. The MS spectra indicate clean formation of Cu(II) loaded oligomers without complications or side reactions of the disulfide bond. An aqueous work-up was performed after each reaction to remove excess copper salt.

3. SAM preparation, analysis and conductive AFM measurements:

Self-assembled monolayer on gold: All glassware employed for monolayer preparation was cleaned with hot "piranha solution", (conc. H_2SO_4-H_2O_2 3:1, **warning**: "piranha solution" should be handled with caution; it reacts strongly in contact with organic compounds), thoroughly rinsed with milliQ water and dried in an oven. For the monolayer formed with asparagusic functionalized foldamers without copper loading, the monolayer was prepared by immersing gold substrates (300 nm Au on mica, Georg Albert PVD – Beschichtungen, Germany) into the stock solutions of the respective compounds for 5 days at room temperature. For the monolayer of the Cu(II) loaded foldamers, the gold substrates were incubated in the stock solutions of the respective Cu(II) loaded asparagusic functionalized foldamers for 15 days at 45 °C. Stock solutions of $AsgQ_n$ (n = 5, 9, 17, 1 mM) and $AsgQ_n \bullet \frac{n-1}{2}Cu$ (n = 5, 9, 17, 0.5 mM) were prepared by dissolving the compounds in degassed $CHCl_3$/EtOH (vol/vol 8:2). The vials for incubation were backfilled with Ar before sealing. Afterwards, the substrates were rinsed with $CHCl_3$ (*ca*. 3 mL), EtOH (*ca*. 3 mL), and dried with a steam of dry Ar. Substrates for PM-IRRAS analysis were prepared with the same procedures using gold substrate squares of *ca*. 2.5 cm sides (200 nm gold on glass, Ssens, Netherlands). All the gold substrates were freshly treated with piranha and then rinsed with milliQ water, ethanol and acetone subsequently. Substrates for conductive AFM analysis were prepared with gold on mica (300 nm Au on mica, Georg Albert PVD – Beschichtungen, Germany), gold substrates on mica were freshly treated by ozone shortly.

Ellipsometry. Ellipsometry measurements were carried out in a EP3 null-ellipsometer

(Nanofilm, Germany) and analyzed with the software (EP4Model 1.0.1) provided with the instrument. The instrument was used in total internal reflection mode and both the intensity and the phase changes of the reflected light were monitored and converted into the ellipsometric angles Ψ and Δ. A wavelength range from 370 to 720 nm was scanned at a constant angle of incidence of 70 ºC. Film thickness was determined by fitting the ellipsometric angles to a built-up model of gold-organic-air. The optical parameters of the gold layer were obtained experimentally by measuring a bare gold substrate. The organic layer was modeled using a Cauchy model assuming a refractive index of 1.4. Results are expressed as the average and standard deviation of three independent monolayer preparations.

***PM-IRRAS*.** PM-IRRAS spectra of $AsgQ_n$ (n = 5, 9, 17) and $AsgQ_n\bullet\frac{n-1}{2}Cu$ (n = 5, 9, 17) were recorded using a ThermoNicolet Nexus 670 FTIR spectrometer at a resolution of 4 cm^{-1} by co-adding several blocks of 1500 scans (30 min acquisition time). Generally, eight blocks (4 h acquisition time) were necessary to obtain PM-IRRAS spectra of SAMs with good signal-noise ratios. Experiments were performed at an incidence angle of 75º by using an external homemade goniometer reflection attachment and adding a ZnSe photoelastic modulator (PEM, Hinds Instruments, type III) after the polarizer.[6] PM-IRRAS spectra are presented in terms of the IRRAS unit (i.e. 1-[Rp(d)/Rp(0)], where Rp(d) and Rp(0) stand for the p-polarized reflectance of the film/substrate and bare substrate systems, respectively) by using a calibration procedure.[6a, 7]

Electrochemistry. Electrochemical measurements were carried out in an Autolab potentiostat (Metrohm, France). Cyclic voltammetry measurements were carried out using a three electrode system: the working electrode, an Ag/AgCl reference electrode and a coiled platinum wire as counter electrode. A Teflon cell was used to define an active circular electrode area of 0.38 cm^2. The working electrodes were the gold substrates modified with SAM of copper loaded $AsgQ_n\bullet\frac{n-1}{2}Cu$ (n = 5, 9, 17) oligomers. The measurements were performed in acetonitrile, 0.1 M of tetrabutylammonium chloride (TBACl) was added as electrolyte, scan rate of 100 mV/s was used.

X-ray photoelectron spectroscopy. Gold substrates functionalized with SAM of the copper loaded $AsgQ_n\bullet\frac{n-1}{2}Cu$ (n = 5, 9, 17) oligomers were prepared as described previously. High-resolution photoemission spectra were recorded using an XPS apparatus (SPECS Surface Nano Analysis GmbH). A photon beam with the energy of 1486.7 eV was generated from an aluminum anode in a microfocus X-ray (XR-MF) source. The XR-MF source was also equipped with a quartz crystal mirror as a monochromator, producing the monochromatic Al K_α X-ray beam. A PHOIBOS 150 Hemispherical Energy Analyzer (HEA) with a nine-single-channel electron multiplier detector (MCD-9) was used to collect photoemission spectra.

***Conducting AFM*.** I-V curves were collected in air with a Dimension Icon AFM (Bruker) in PeakForce TUNA mode using PFTUNA tips (Bruker, platinum/iridium tip, nominal parameters: radius, 25 nm; spring constant, 0.4 N/m,). Substrates were grounded with a metal wire in contact with the gold surface. The tip spring constant was calibrated in order to calculate the applied force. Junctions were established at gentle tip pressures by defining 9 points distributed in a ca 2500 nm^2 area using the instrument's “point-and-shoot” feature. Forward and reverse currents were measured by triplicate in each point. Data was collected from several different areas on the sample and at different tip pressures. The same tip was employed to measure different monolayers to avoid differences arising from variable tip diameter. Comparative experiments were repeated with different tips.

A non-ohmic response is generated as the system is composed of a semiconductor sandwiched between two metal contacts. The values of the resistance (or conductivity) are taken from the slope at low bias where the behavior is linear as described by Wold & Frisbie.[8] Only those results that gave open circuit or shorts were excluded and we did not ignore values that deviate far from the mean. For this reason, the values contain substantial scatter, but we believe that this is in the nature of these delicate experiments.

4. Magnetic susceptibility measurements

Magnetic susceptibility measurements were performed on a Quantum Design SQUID MPMS-XL magnetometer housed at the Transform Platform of the Centre de Recherche Paul Pascal (CNRS – Univ. Bordeaux, France) at temperatures between 1.8 and 300 K and *dc* magnetic fields up to +7 T. The measurements were carried out on polycrystalline samples of **Q_5•2Cu** and **Q_7•3Cu** (15.23 and 16.21 mg, respectively) introduced in a sealed polyethylene bag (3 × 0.5 × 0.02 cm; 11.20 and 10.97 mg respectively). Prior to the experiments, the field-dependent magnetization was measured at 100 K to exclude the presence of bulk ferromagnetic impurities. In fact, paramagnetic or diamagnetic materials should exhibit a perfectly linear dependence of the magnetization that extrapolates to zero at zero *dc* field; the sample appeared to be free of any significant ferromagnetic impurities. The magnetic susceptibilities were corrected for the sample holder and the intrinsic diamagnetic ($-0.5 \times MW \times 10^{-6}$ cm^3/mol) contributions.

The susceptibility measurements were performed in temperature at 1000 Oe and 10000 Oe (Figures S21, S22). For both compounds, the χT product is constant for temperatures above 30 K (χT = 0.82 and 1.16 cm^3 K/mol for **Q_5•2Cu** and **Q_7•3Cu**, respectively, at 300 K). This behavior is in good agreement with the presence of two and three paramagnetic S = 1/2 Cu(II) centers (and Curie Constants C = 0.75 and 1.125 cm^3 K/mol, respectively, with g = 2). At lower temperature, the χT product increases up to 0.97 and 1.44 cm^3 K/mol, for **Q_5•2Cu** and **Q_7•3Cu**, respectively, at 1.85 K under an applied magnetic field of 1000 Oe. This thermal behavior suggests the presence of dominating ferromagnetic exchange between S = 1/2 Cu centers.

Magnetic field, H, dependence of the magnetization, M, has been also measured at 1.85 K up to 7 T (Figures S21, S22). For both compounds, the magnetization is increasing rapidly before reaching a clear saturation at high field with a saturation value around 2.12 and 3.02 μ_B for **Q_5•2Cu** and **Q_7•3Cu**, respectively. This field behavior is in agreement with the expected magnetization values: $M_{theoretical}$ = 2 and 3 μ_B for two and three S = 1/2 spins and g = 2.

In order to estimate ferromagnetic interactions, the full set of magnetic data (susceptibility as a function of the temperature and magnetization as a function of the applied magnetic field) has been fitted numerically with the PHI software.[9] As shown in Figures S21 and S22, experimental magnetic data can be fully reproduced using an isotropic Heisenberg spin Hamiltonian considering either two or three S = 1/2 centers for **Q_5•2Cu** and **Q_7•3Cu**, respectively: $\boldsymbol{H} = -2J\, \boldsymbol{S}_A \cdot \boldsymbol{S}_B$ and $\boldsymbol{H} = -2J\, (\boldsymbol{S}_A \cdot \boldsymbol{S}_B + \boldsymbol{S}_B \cdot \boldsymbol{S}_C)$ for **Q_5•2Cu** and **Q_7•3Cu**, respectively. The best set of parameters is g = 2.10(5) and 2.03(5) and J/k_B = +0.85(8) and +0.78(8) K respectively.

5. Crystallography

Single crystals suitable for x-ray diffraction analysis were obtained by slow solvent evaporation from chloroform/methanol mixtures. For Q_5•2Cu, Q_7•3Cu and Q_9•4Cu, the dark solid was dissolved into a small amount of $CHCl_3$. Methanol was carefully added until a precipitate started to form. Then one or few more drops of $CHCl_3$ were added to obtain a clear solution. The vial containing the solution was capped and kept at room temperature avoiding any turbulence. A small hole was made with a needle in the cap to allow slow evaporation of

solvents. Q_7•2Cu crystals were obtained after working up the reaction without removing the acetic acid generated during the reaction. Q_7•xCu crystals of a mixture of different loading of Cu(II) was obtained by mixing Q_7 and 1 equivalent of $Cu(OAc)_2$ in $CHCl_3$/MeOH and let slowly evaporating the solvent at room temperature. The crystal $(Q_3•Zn)_2$ were obtained by mixing Q_3 and $Zn(OAc)_2$ (1 to 1 ratio) at room temperature and letting the sample under slow evaporation of solvents. Crystals gew after around 1 week.

The X-ray diffraction measurements for all crystals were carried out on a Rigaku FRX rotating anode (2.9 kW) diffractometer at the IECB x-ray facility (UMS 3033 – UMS001). CuKα radiation monochromated with high flux Osmic Varimax mirrors was used for data collection. The x-ray source is equipped with a Dectris Pilatus 200K detector and partial chi goniometer. All crystals were kept at 100(2) K during data collection. The Rigaku CrystalClear suite[10] was used to index and integrate data with a multi-scan absorption correction. Structures **$(Q_3•Zn)_2$**, **Q_5•2Cu**, **[Q_7•3Cu+ 2(Q_7•2Cu) + Q_7•Cu]** were solved with the ShelXT[11] structure solution program using Intrinsic Phasing, while structures **Q_7•2Cu**, **Q_7•3Cu** and **Q_9•4Cu** were solved by direct methods with SIR2014[12]. With Olex2,[13] the structures were refined with the ShelXL[14] refinement package using Least Squares minimization.

In all structures, backbones were refined with anisotropic displacement parameters except a disordered part of the main chain of **Q_7•3Cu**. Anisotropic displacement parameters for side chains and solvent molecules were introduced whenever it was possible. Different approaches have been used for hydrogen atoms, depending on the data quality: a) H atoms were localized on electron density maps, b) H atoms were placed geometrically, c) no H atoms were localized. All H atoms were constrained depending on their environment and were refined in the riding-model approximation, with Uiso(H)=1.2Ueq(CH, CH2, NH) and Uiso(H)=1.5Ueq(CH_3, OH).

DFIX, AFIX, FLAT, EADP, RIGU and DELU instructions were employed to model the molecules' geometry and temperature parameters. The **Q_7•3Cu** structure was refined as an inversion twin.

Heavily disordered solvent molecules in **Q_7•2Cu**, **Q_7•3Cu** and [**Q_7•3Cu+ 2(Q_7•2Cu) + Q_7•Cu**] were removed using the SQUEEZE[15] procedure. For search and analysis of solvent-accessible voids in the structures, default parameters were used: grid 0.20 Å, probe radius 1.2 Å and NStep 6. Calculated total potential solvent-accessible void volumes and electron counts per unit cell were 2346 $Å^3$ and 740, 1780 $Å^3$ and 421, 3986 $Å^3$ and 765 for **Q_7•2Cu, Q_7•3Cu and** [**Q_7•3Cu+ 2(Q_7•2Cu) + Q_7•Cu**], respectively.

The refinement of the foldamer crystal structures faced problems usually observed in macromolecules crystallography, *i.e.* large volume fractions of disordered solvent molecules, weak diffraction intensity, incompleteness of the data, moderate or low resolution. Thus it is not surprising that a number of A-level and B-level alerts were detected using IUCR's checkcif algorithm. These alerts are inherent to the data and refinement procedures and do not reflect errors. They are listed below and have been divided into two groups.

Group 1 alerts illustrate the poor quality of the data and refinement statistics if compared to that expected for small molecule structures from highly diffracting crystals:

THETM01_ALERT_3_B The value of sine(theta_max)/wavelength is less than
PLAT023_ALERT_3_B Resolution (too) Low [sin(theta)/Lambda < 0.6]..
PLAT029_ALERT_3_B _diffrn_measured_fraction_theta_full value Low
PLAT082_ALERT_2_A High R1 Value
PLAT084_ALERT_3_B High wR2 Value (i.e. > 0.25)
PLAT220_ALERT_2_B Non-Solvent Resd 1 C Ueq(max)/Ueq(min) Range
PLAT230_ALERT_2_B Hirshfeld Test
PLAT234_ALERT_4_B Large Hirshfeld Difference
PLAT241_ALERT_2_B High 'MainMol' Ueq as Compared to Neighbors of
PLAT242_ALERT_2_B Low 'MainMol' Ueq as Compared to Neighbors of

PLAT341_ALERT_3_B Low Bond Precision on C-C Bonds
PLAT910_ALERT_3_B Missing # of FCF Reflection(s) Below Theta(Min).
PLAT934_ALERT_3_A Number of (Iobs-Icalc)/Sigma(W) > 10 Outliers
PLAT973_ALERT_2_B Check Calcd Positive Resid. Density on Cu2

Group 2 is connected with the decision made during refinement and explained below:

PLAT043_ALERT_1_B Calculated and Reported Mol. Weight Differ
Not all H atoms were determined, but they were used in SFAC calculation

PLAT201_ALERT_2_A Isotropic non-H Atoms in Main Residue(s)
PLAT202_ALERT_3_A Isotropic non-H Atoms in Anion/Solvent
As indicated above, not all non-H atoms were refined with anisotropic displacement parameters.

PLAT306_ALERT_2_B Isolated Oxygen Atom (H-atoms Missing ?)
Unrecognized electron density was introduced to the refinement as dummy oxygen atoms

PLAT326_ALERT_2_B Possible Missing H on sp3? Carbon
PLAT315_ALERT_2_B Singly Bonded Carbon Detected (H-atoms Missing)
As indicated above, not all H atoms were determined.

PLAT430_ALERT_2_B Short Inter D...A
The position of solvent molecules is poorly determined

PLAT601_ALERT_2_B Structure Contains Solvent Accessible VOIDS of
Not all electron density could be reasonably modelled thus, in the structures, solvent-accessible voids are observed.

PLAT987_ALERT_1_B The Flack x is >> 0 - Do a BASF/TWIN Refinement
The structure was refined as an inversion twin.

Table S1: Crystallographic data

Identification code	**$(Q_3•Zn)_2$**	**$Q_5•2Cu$**	**$Q_7•2Cu$**
Chemical formula	$2(C_{43}\ H_{42}\ N_6\ O_9\ Zn),\ 7(CH_3OH)$	$2(C_{71}H_{68}Cu_2N_{10}O_{13})\cdot 2(H_2O)\cdot\ 4.187(CHCl_3)\ 0.278(O)^*\cdot$	$C_{99}H_{96}Cu_2N_{14}O_{17}\cdot 0.232(CH_3OH)$
Formula weight	1928.68	3332.53	1888.34
Crystal system	Triclinic	Monoclinic	Triclinic
Space group	*P*-1	$P2_1/c$	*P*-1
Unit cell dimensions (Å,°)	a=14.7656 (13), α=78.758 (5) b=17.8143 (12), β=84.709 (7) c=18.0099 (10), γ=87.695 (9)	a=19.931 (4), α=90 b=23.856 (5), β=92.62 (3) c=31.160 (6), γ=90	a=17.611 (2), α=102.059 (6) b=19.895 (3), β=102.050 (5) c=32.618 (6), γ=95.906 (3)
Volume ($Å^3$)	4625.4 (6)	14800 (5)	10801 (3)
Z	2	4	4
Density (calculated, Mg m^{-3})	1.385	1.496	1.161
Absorption coefficient	1.33	3.39	1.02
Crystal size	0.30 × 0.10 × 0.04	0.30 × 0.07 × 0.03	0.30 × 0.03 × 0.01
Index ranges	h = -17→15, k = -21→21, l = -21→21	h = -24→17, k = -29→27, l = -38→35	h = -19→21, k = -23→23, l = -39→39
Completeness/$theta_{full}$ (°)	98.6/67.68	95.3/67.68	97.1/67.8
Reflections collected	65265	63583	140155
Reflections observed [$I > 2\sigma(I)$]	15081	17346	29906
R_{int}	0.025	0.074	0.055
Data/parameters/restrains	16700/1240/0	27285/2017/166	38424/2382/35
Goodness-of-fit on F^2	1.09	1.29	1.03
Final R indices [$I > 2\sigma(I)$]	R1 = 0.0433, wR2 = 0.1143	R1 = 0.1136, wR2 = 0.3338	R1 = 0.0797, wR2 = 0.2247
R indices (all data)	R1 = 0.0471, wR2 = 0.1161	R1 = 0.1467, wR2 = 0.3614	R1 = 0.0956, wR2 = 0.2393
Lasgest diff. peak and hole	0.79, -0.61	1.49, -2.07	1.14, -0.59
CCDC #	2074374	2074375	2074377

*Unrecognized electron density was introduced to the refinement as dummy oxygen atoms.

Data collections were performed at 100K using CuKα radiation. Multi-scan absorption correction was introduce.

Table S1: Crystallographic data (continued from previous page)

Identification code	**Q_7•3Cu**	**Q_7•3Cu+ 2(Q_7•2Cu) + Q_7•Cu**	**Q_9•4Cu**
Chemical formula	$C_{99}H_{87}Cu_3N_{14}O_{17}$·2($CH_4O$)·3(O)·1.5($CHCl_3$) 3(O)*·	$C_{99}H_{97.44}N_{14}O_7Cu_{1.28}$·$C_{99}H_{97.76}N_{14}O_7Cu_{1.12}$·$C_{99}H_{97.2}N_{14}O_7Cu_{1.4}$·$C_{99}H_{98}N_{14}O_7Cu$·1.3($CHCl_3$)·$CH_4O$·10.7(O)*	$C_{127}H_{120}N_{18}O_{21}Cu_4$·3($CHCl_3$)
Formula weight	2226.58	7045.43	2846.67
Crystal system	Orthorhombic	Triclinic	Monoclinic
Space group	*P*na2_1	*P*-1	*P*2_1
Unit cell dimensions (Å,°)	a=20.159 (4), α=90 b=24.589 (5), β=90 c=43.858 (11), γ=90	a=20.951 (3), α=61.86 (3) b=33.872 (3), β=73.72 (4) c=35.0813 (18), γ=76.66 (4)	a=13.5862 (17), α=90 b=26.752 (4), β=91.941 (6) c=17.989 (2), γ=90
Volume (Å^3)	21740 (8)	20929 (8)	6534.3 (15)
Z	8	2	2
Density (calculated, Mg m^{-3})	1.361	1.118	1.447
Absorption coefficient	2.31	1.04	3.04
Crystal size	0.20 × 0.07 × 0.04	0.10 × 0.05 × 0.01	0.20 × 0.15 × 0.02
Index ranges	*h = -24→24, k = -29→29, l = -52→52*	*h = -23→23, k = -37→37, l = -38→38*	*h = -15→14, k = -31→30, l = -21→15*
Completeness/theta$_{full}$ (°)	99.9/67.68	97.4/58.94	98.1/65.1
Reflections collected	153656	223502	37709
Reflections observed [$I > 2\sigma(I)$]	33443	26446	14687
R_{int}	0.065	0.087	0.039
Data/parameters/restrains	39451/2040/161	58565/3203/816	19145/1397/135
Goodness-of-fit on F^2	1.49	2.06	1.00
Final R indices [$I > 2\sigma(I)$]	R1 = 0.1312, wR2 = 0.3551	R1 = 0.2388, wR2 = 0.5663	R1 = 0.0876, wR2 = 0.2362
R indices (all data)	R1 = 0.1384, wR2 = 0.3726	R1 = 0.3072, wR2 = 0.6126	R1 = 0.1013, wR2 = 0.2483
Lasgest diff. peak and hole	2.10, -0.98	1.27, -0.72	1.16, -0.88
CCDC #	2074378	2074376	2074379

*Unrecognized electron density was introduced to the refinement as dummy oxygen atoms.

Data collections were performed at 100K using CuKα radiation. Multi-scan absorption correction was introduce.

6. Additional Figures:

6.1 UV-Vis titration of Q_n with Cu(II)

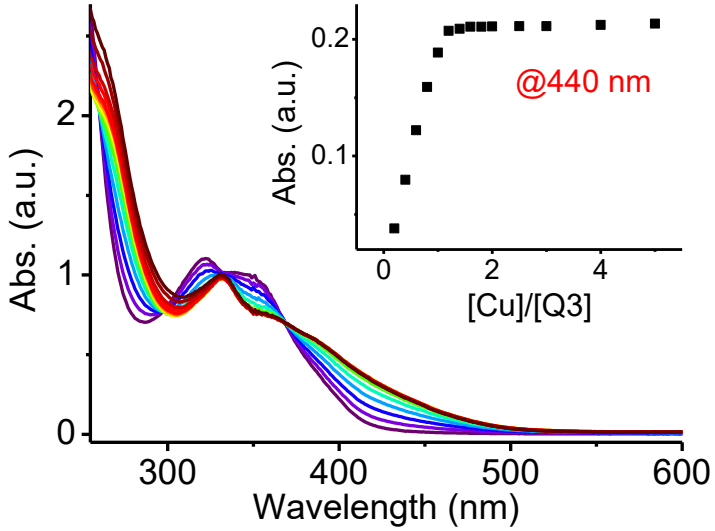

Figure S1: UV-Vis titration of $Cu(OAc)_2$ into Q_3, $[Q_3] = 5\times10^{-5}$ M, solvent: $CHCl_3$/MeOH (1:1, vol/vol), the inset shows the evolution of absorbance at 440 nm upon addition of $Cu(OAc)_2$.

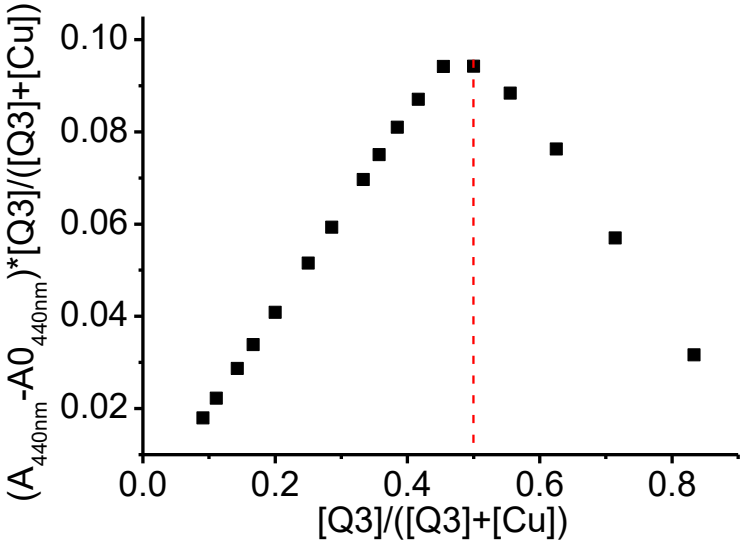

Figure S2: Job's plot of the association of Q_3 and Cu(II) indicating that the binding stoichiometry is 1:1.

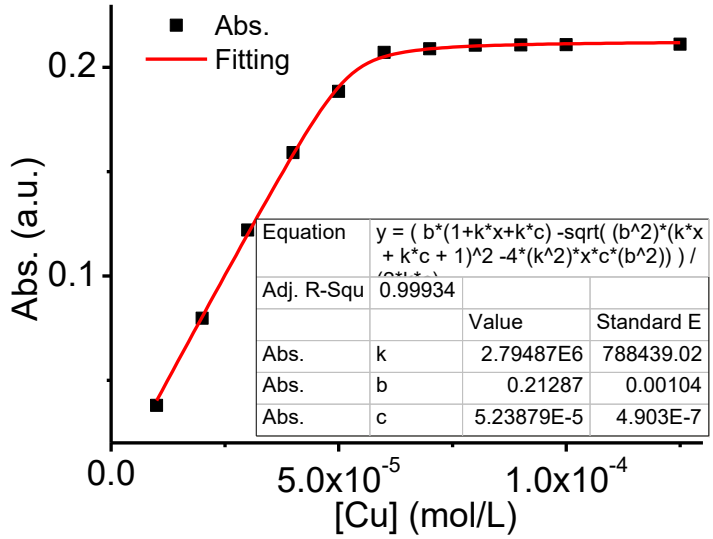

Figure S3: nonlinear fitting curve of the absorbance at 440 nm. The fitting equation was based on a 1 1 binding isotherm. An estimate of $K > 2.8\times10^{6}$ L^{-1} mol^{-1} was obtained.

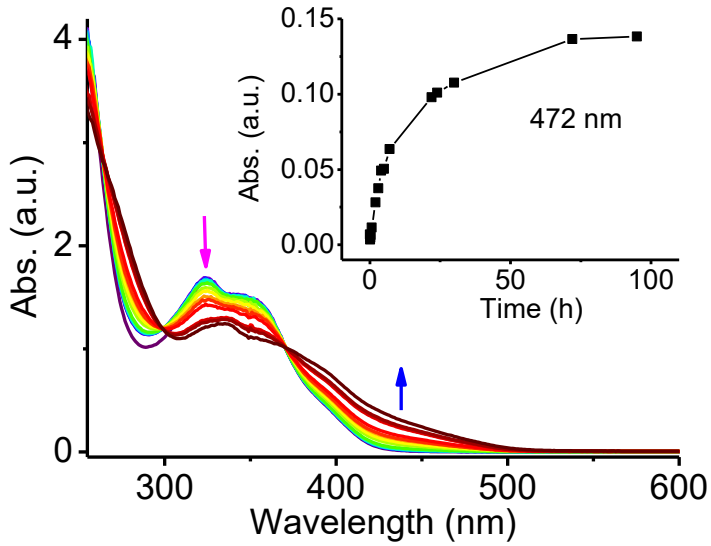

Figure S4: Kinetics of the formation of the Cu(II) complex of Q_5 at room temperature in $CHCl_3$/MeOH (vol/vol 1:1)followed by UV-Vis spectroscopy. The inset shows changes of absorbance at 472 nm with time. $[Q_5] = 5\times10^{-5}$ M, $[Cu] = 1\times10^{-4}$ M.

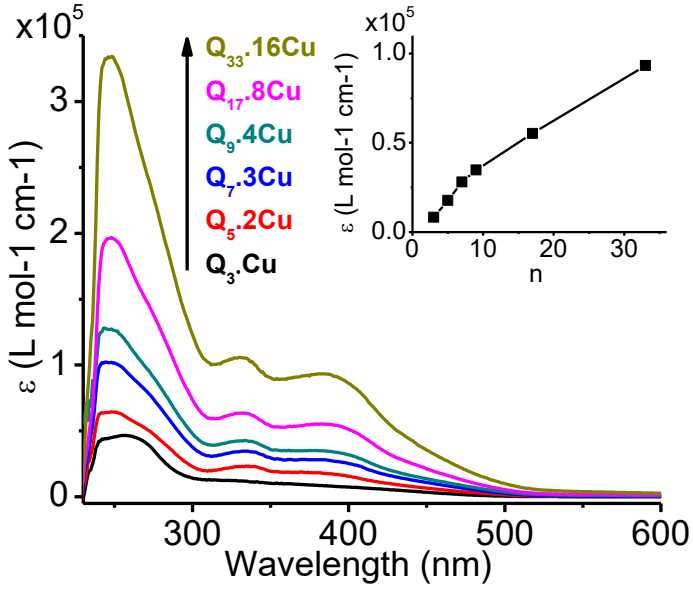

Figure S5: UV-Vis spectra of Q_3•Cu, Q_5•2Cu, Q_7•3Cu, Q_9•4Cu, Q_{17}•8Cu and Q_{33}•16Cu. All the spectra were measured in $CHCl_3$ at room temperature. The inset shows the absorbance at 385 nm of the copper loaded oligomers as a function of the number of quinoline units.

6.2 ESI+ MS of Cu(II) loaded Q_n (n = 3, 5, 7, 9, 17, 33) and $AsgQ_n$ (n = 5, 9, 17)

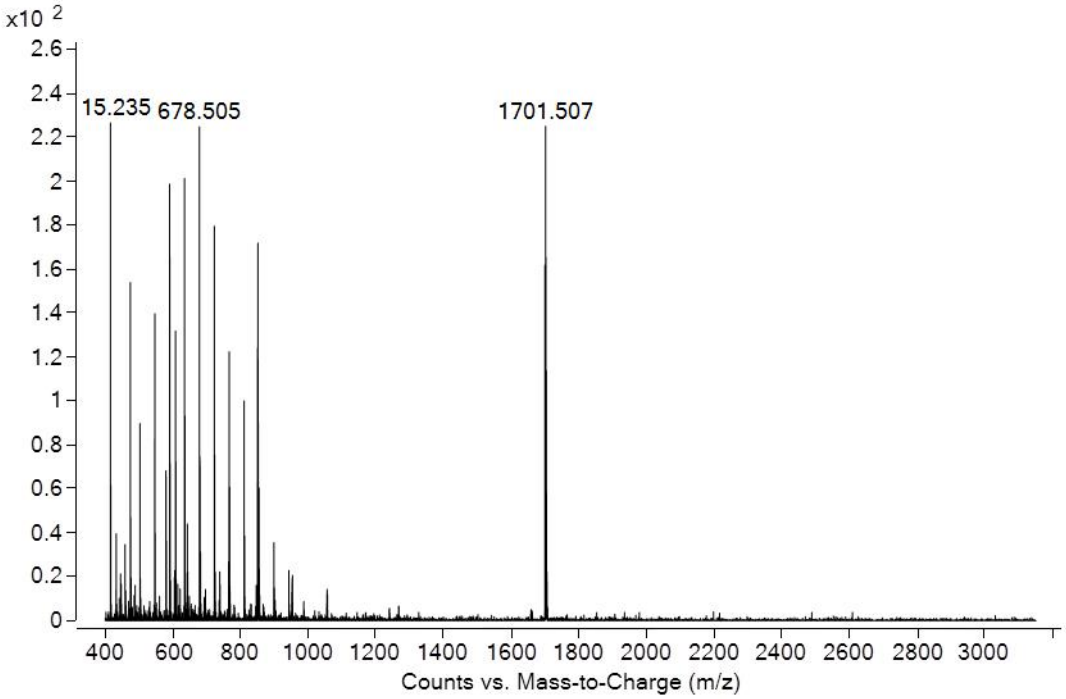

Figure S6: ESI+ HRMS of Q_3•Cu.

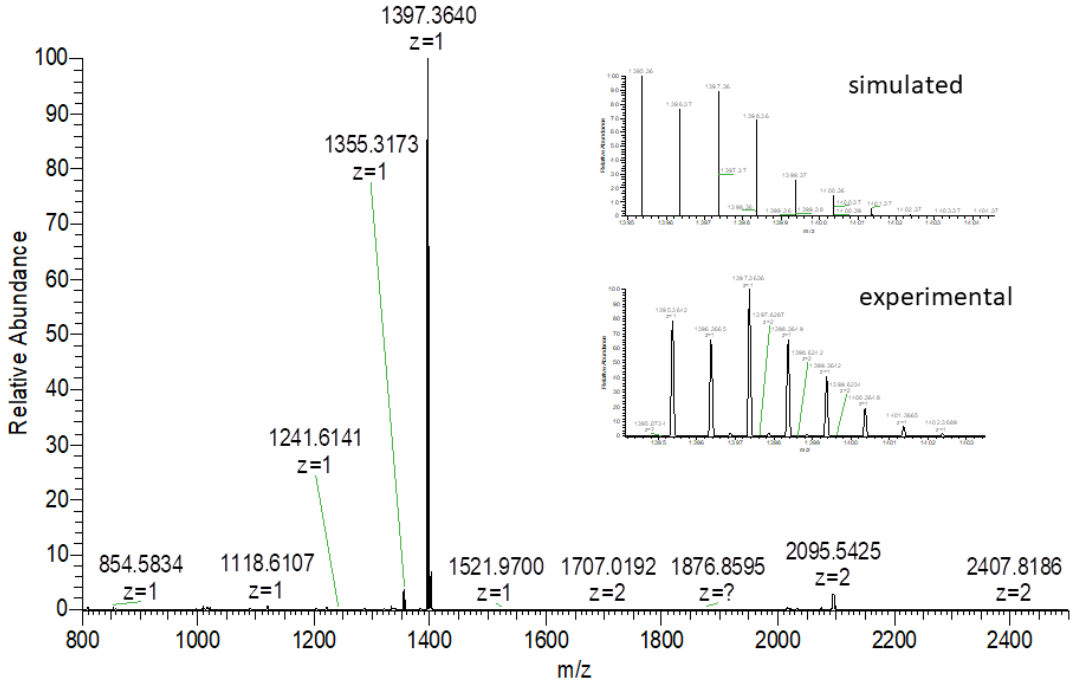

Figure S7: ESI+ HRMS of Q_5•2Cu. The inset shows the calculated (top) and experimental (bottom) isotope distribution of molecular ions.

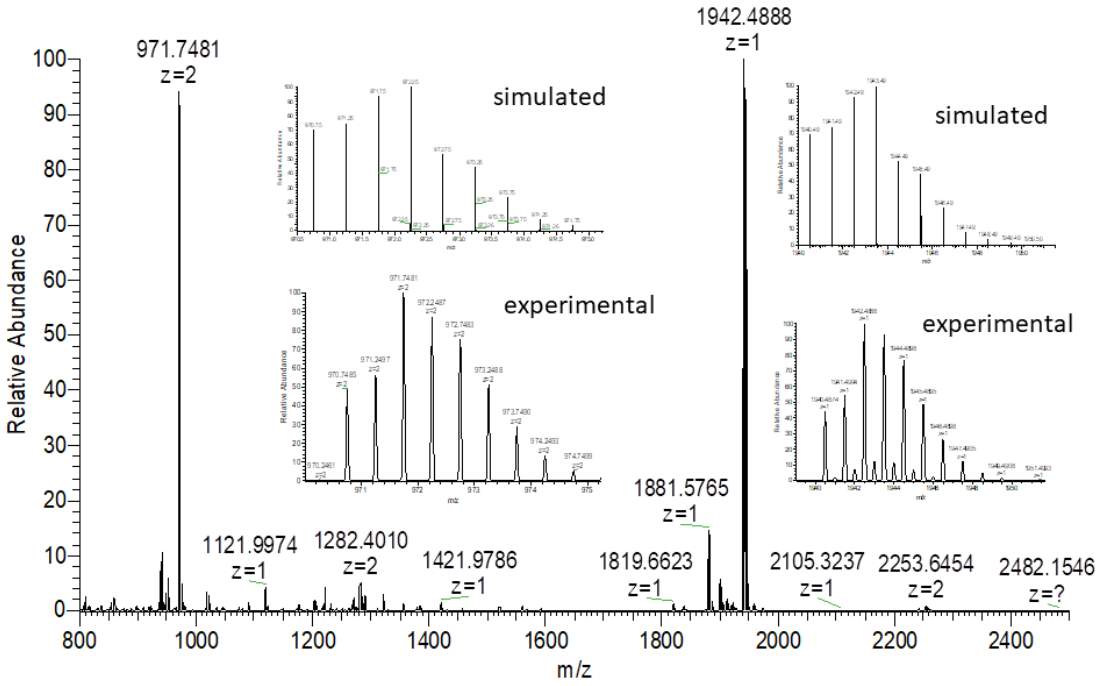

Figure S8: ESI+ HRMS of Q_7•3Cu. Insets show the calculated (top) and experimental (bottom) isotope distribution of molecular ions for Z = 2 (left) and Z = 1 (right).

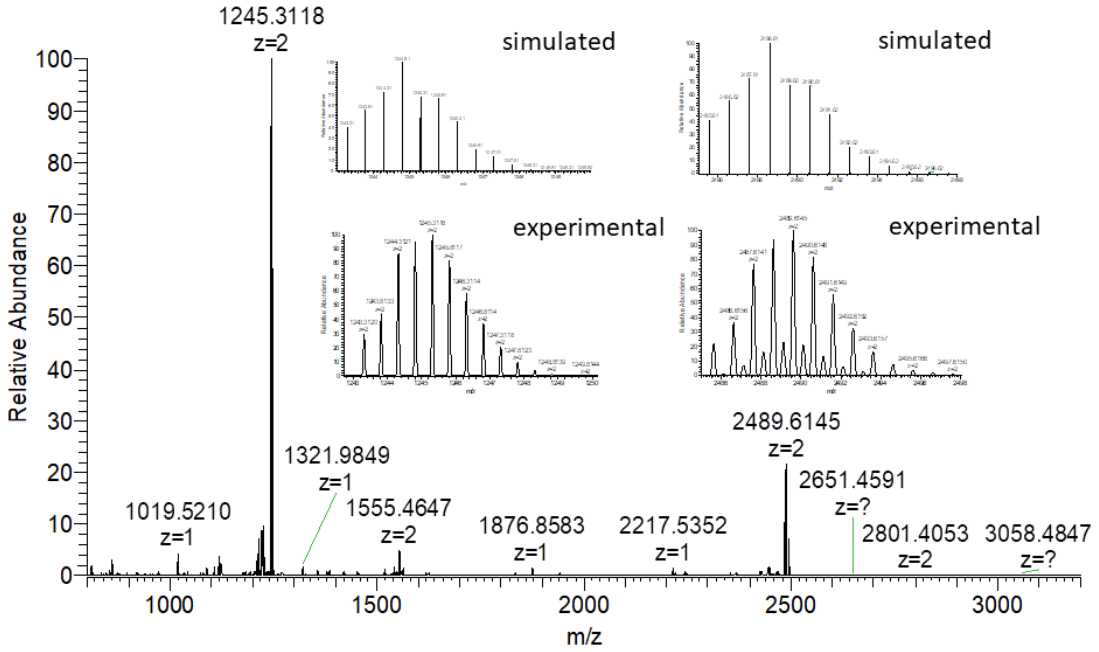

Figure S9: ESI+ HRMS of Q_9•4Cu. Insets show the calculated (top) and experimental (bottom) isotope distribution of molecular ions for Z = 2 (left) and Z = 1 (right).

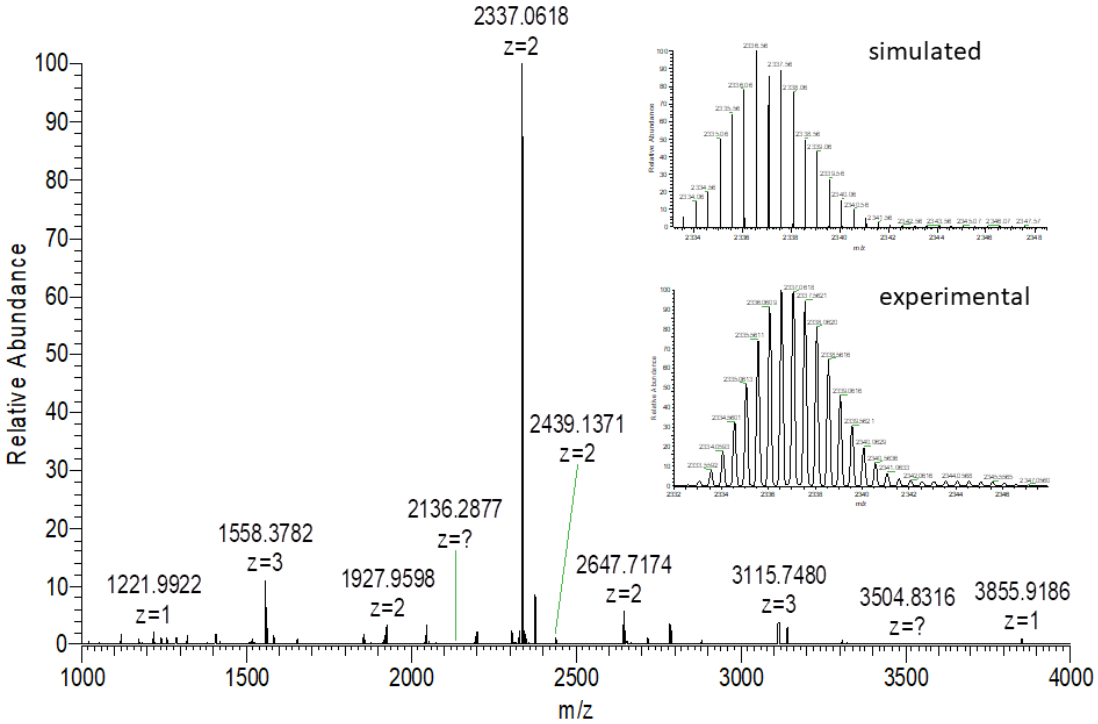

Figure S10: ESI+ HRMS of Q_{17}•8Cu. The inset shows the calculated (top) and experimental (bottom) isotope distribution of molecular ions.

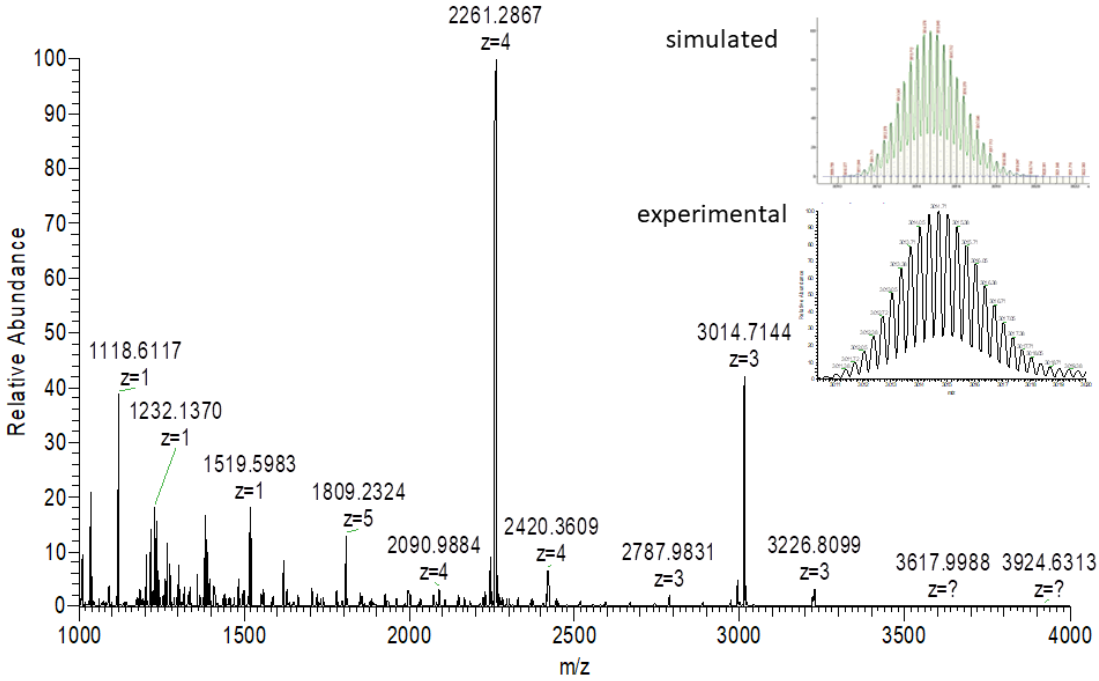

Figure S11: ESI+ HRMS of Q_{33}•16Cu. The inset shows the calculated (top) and experimental (bottom) isotope distribution of molecular ions.

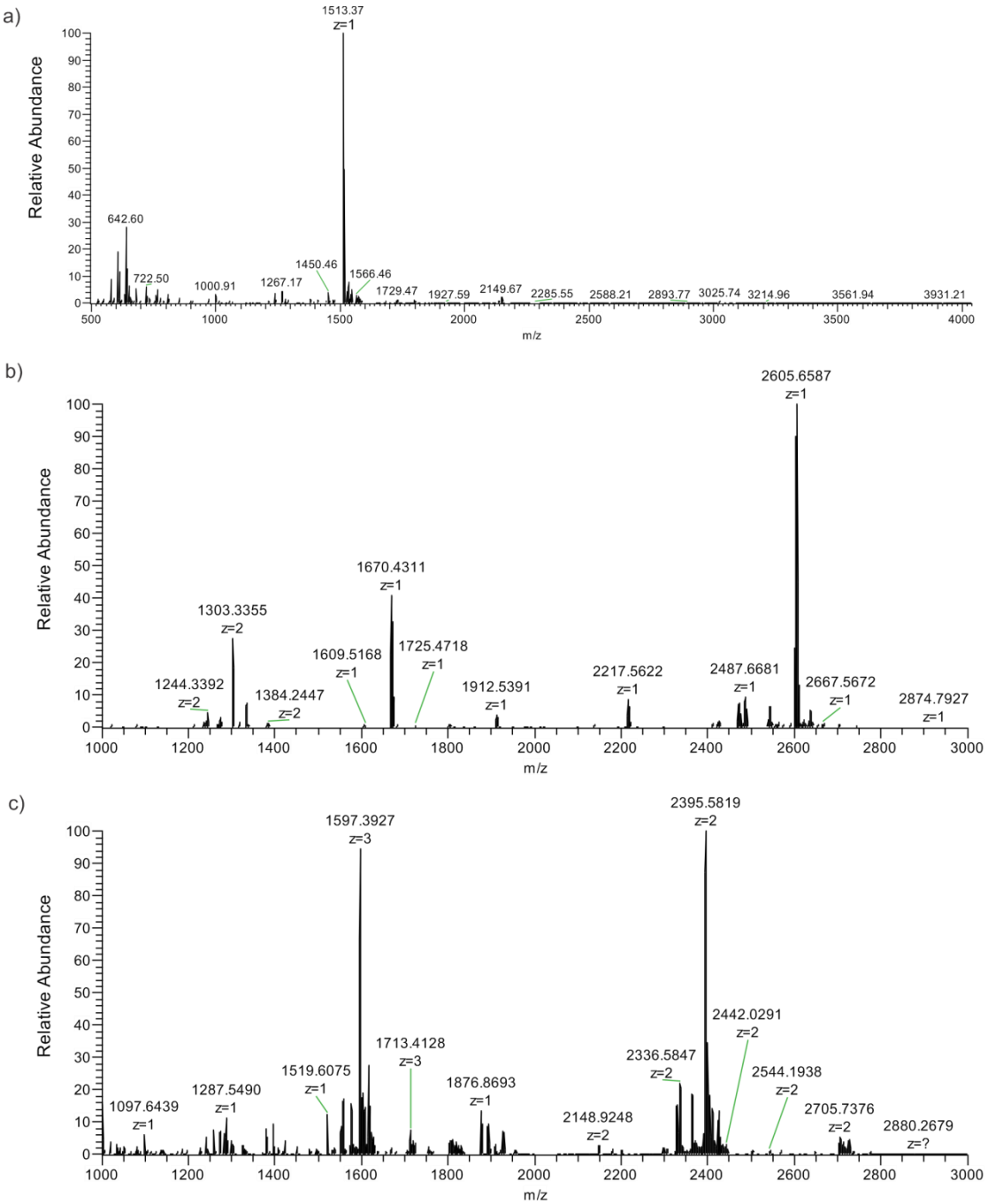

Figure S12: ESI+ MS spectra of a) $AsgQ_5$•2Cu; b) $AsgQ_9$•4Cu; c) $AsgQ_{17}$•8Cu. In all three MS spectra, all the highest peaks correspond to the target product. In the spectra c), both 2+ and 3+ ions were observed.

6.3 Q_3 complexation with Pd(II) and Zn(II)

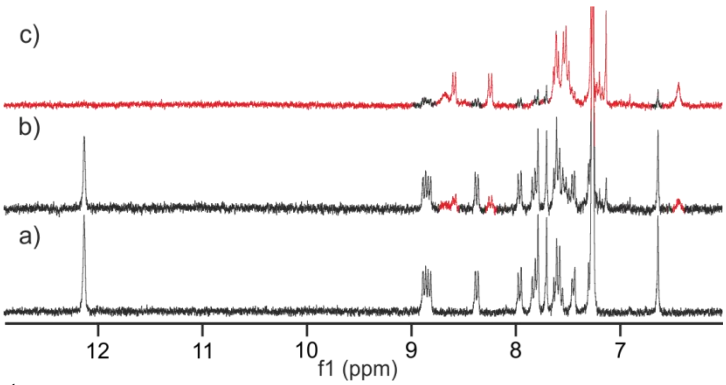

Figure S13: Part of ^{1}H NMR (300 MHz) spectra of a) Q_3, and Q_3 mixed with 1 equiv. of $Pd(OAc)_2$ standing at r.t. for b) 4 hours and c) 7 days. [Q_3] = 1 mM in $CDCl_3$/MeOD-D_4 (8:2, vol/vol).

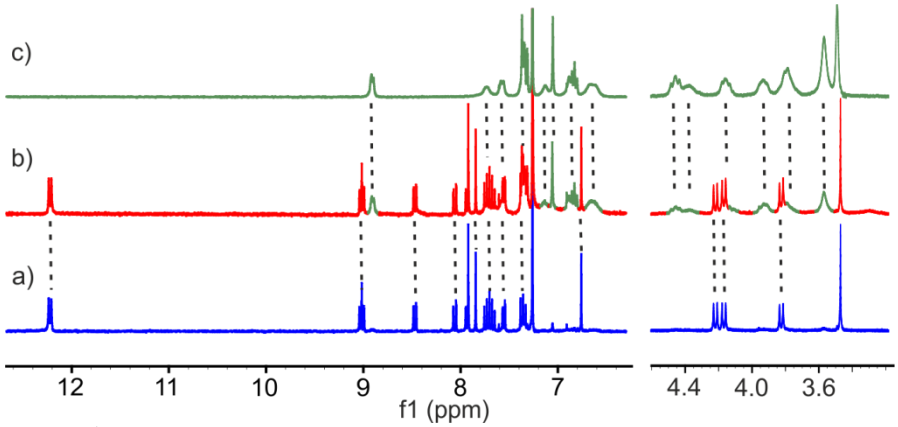

Figure S14: Part of ^{1}H NMR (300 MHz) spectra of a) Q_3; b) Q_3 mixed with 1 equiv. of $Zn(OAc)_2$ at room temperature after 16 hours; c) freshly dissolved crystals of the Q_3•Zn complex. The solvent is $CDCl_3$ for all three spectra.

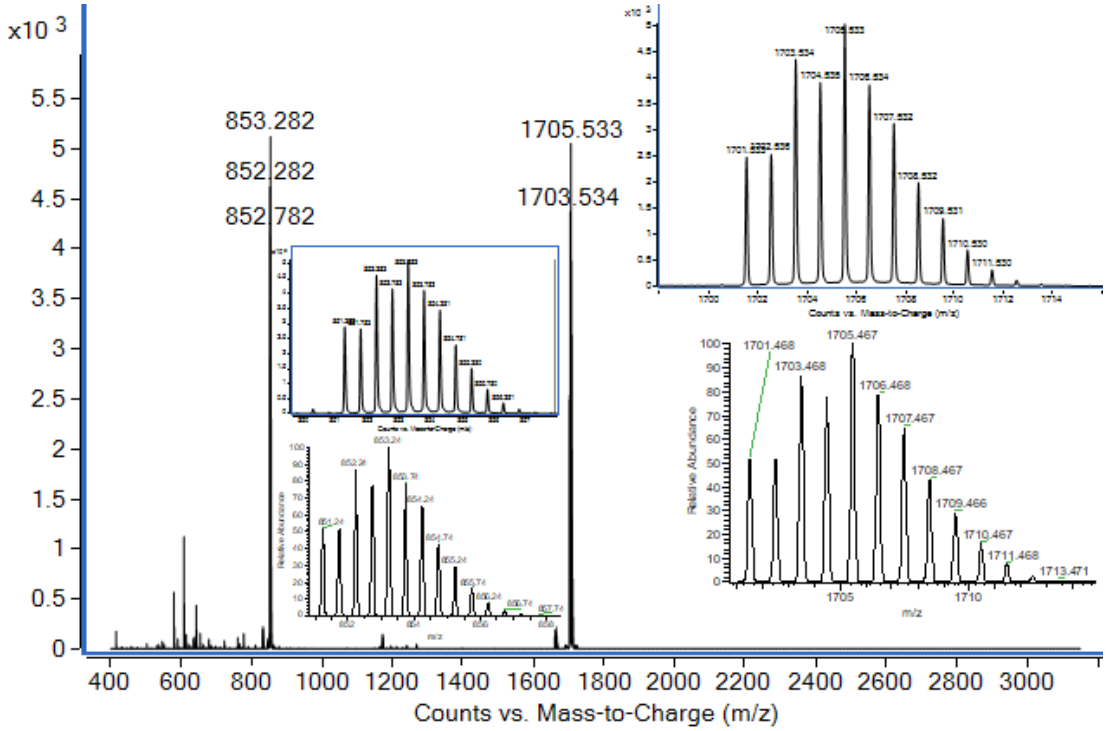

Figure S15: ESI+ HRMS of Q_3•Zn complex. The insets show the experimental (top) and calculated (bottom) isotope distributions for z=2 and z=1 molecular ions

.

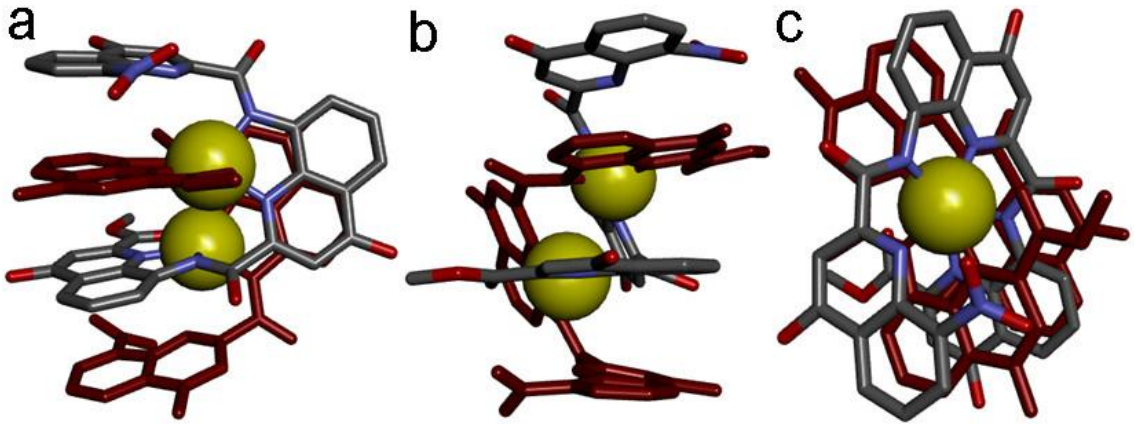

Figure S16: Crystal structure of Q_3•Zn. a) side view, b) front view and c) top view. The Zn atoms are showed in space filling models. All hydrogen atoms and side chains were removed for clarity.

6.4 Other figures of Cu(II) loaded Q_n oligomers

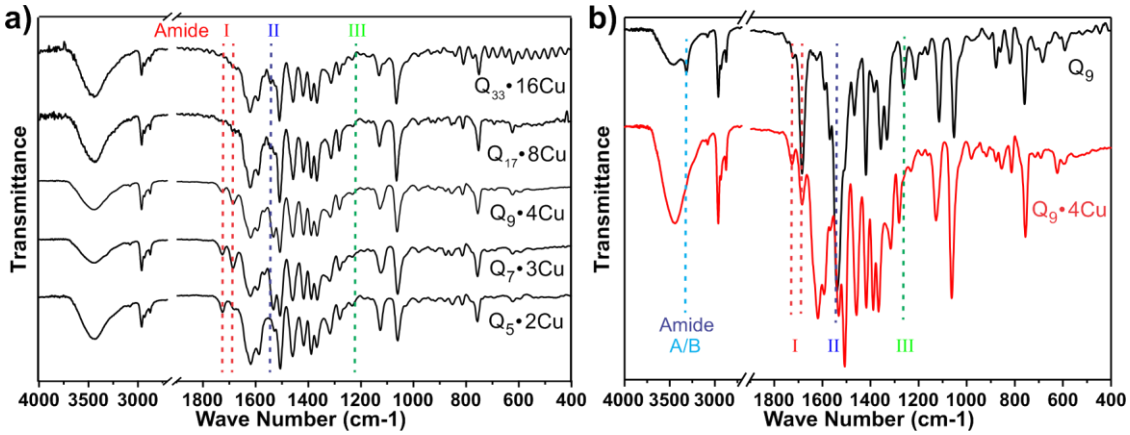

Figure S17: a) FTIR spectra (transmittance) ofQ_5•2Cu, Q_7•3Cu, Q_9•4Cu, Q_{17}•8Cu and Q_{33}•16Cu. B) comparison of the FTIR spectra of Q_9•4Cu and Q9 showing the shift of the Amide I, and the disappearance of the amide A/N and Amide III bands upon Cu(II) complexation.

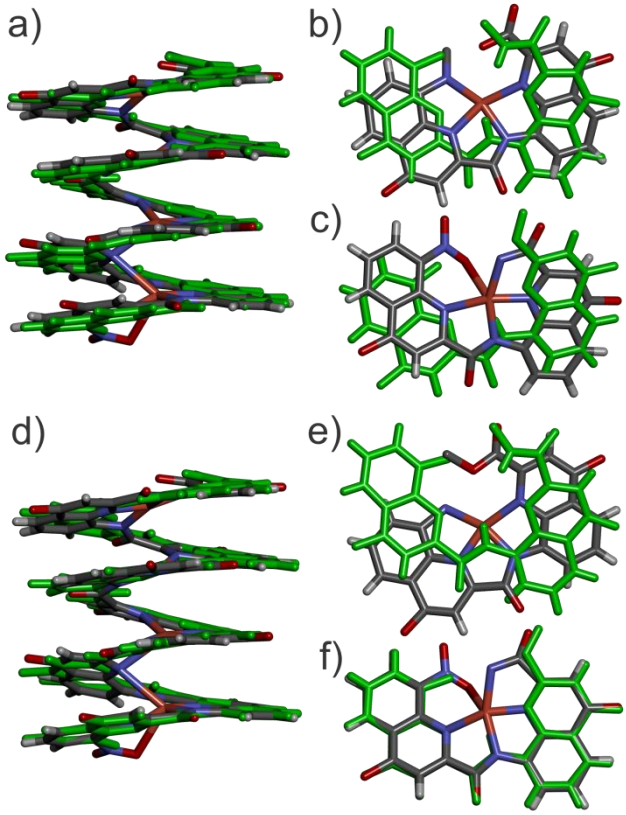

Figure S18: Overlay of the crystal structures of Q_9 and Q_9•4Cu. Showing: a) overlay of the entire helix backbone; b) the C-terminal last two units of the overlay in a); c) the N-terminal last two units of the overlay in a); d) overlay of the two N-terminal quinoline rings; e) the C-terminal last two units of the overlay in d); c) the N-terminal last two units of the overlay in d). Side chains were removed for clarity.

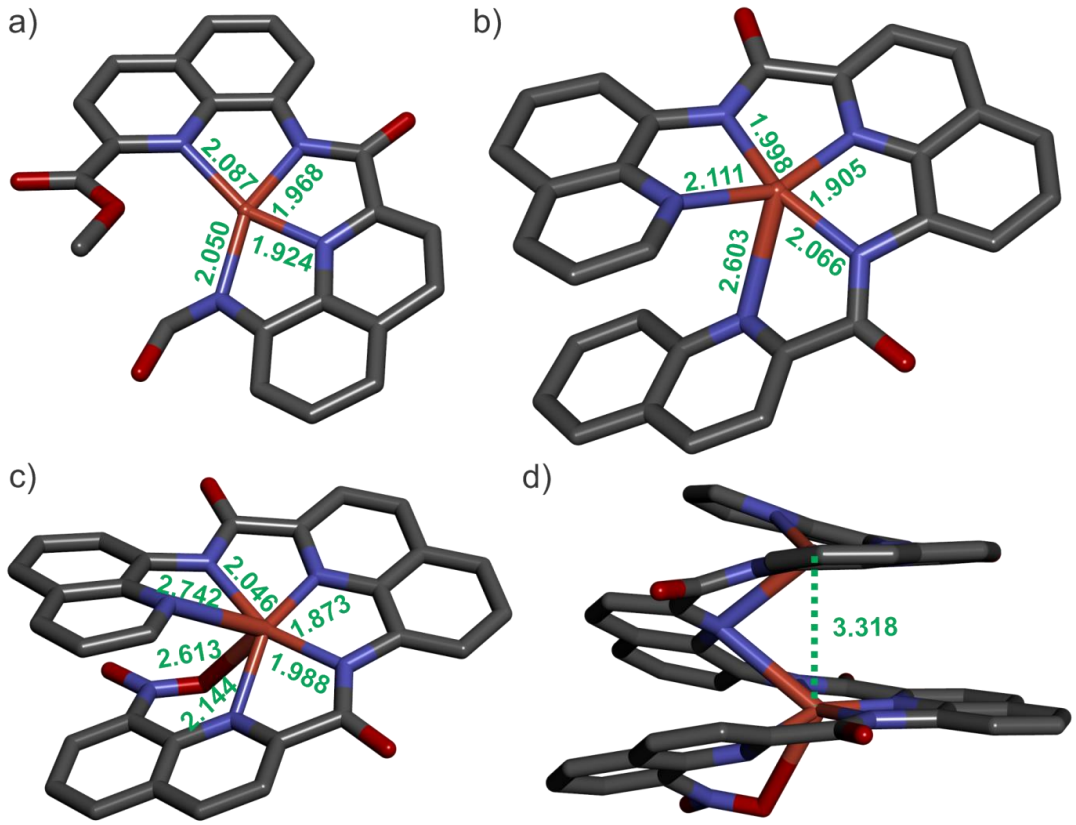

Figure S19： Examples of Cu(II) centers in the structure of Q_9•4Cu that are four- (a), five- (b) or six-coordinate (c). d) Example of a quinoline ligand that bridges two Cu(II) centers, the number indicate the distance between the two Cu(II) centers in Å. The numbers indicate atomic distances in Å.

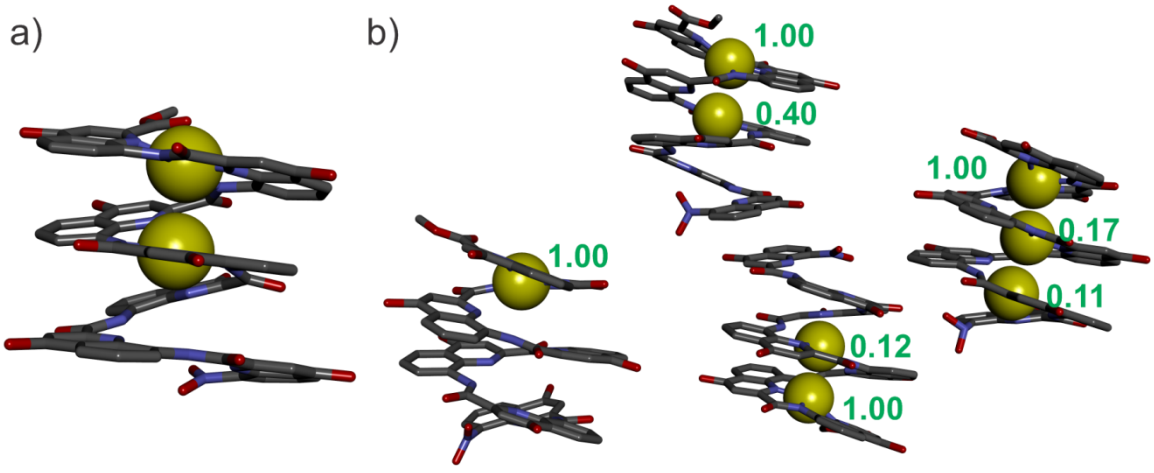

Figure S20: a) Single crystal structure of Q_7•2Cu; b) the crystal structure of partially copper loaded Q_7 showing four independent complexes with 1, 2 or 3 partially occupied copper ions in the asymmetric unit cell. The numbers next the Cu(II) centers indicate the occupancy factors, the values were deduced from fitting electron density and are not very accurate. All side chains and hydrogen atoms were removed for clarity.

6.5 Magnetic susceptibility

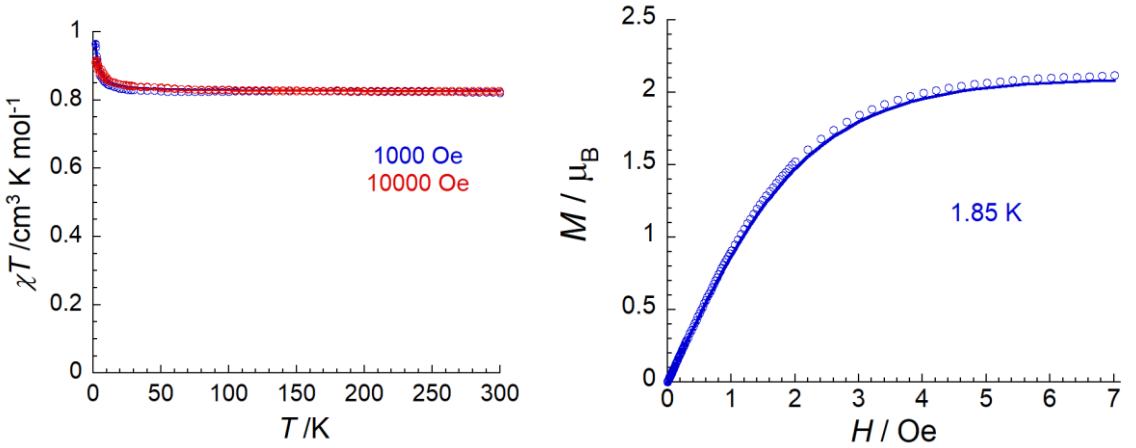

Figure S21: Left: Temperature dependence of the dc susceptibility, χ (defined as M/H per complex), shown as a χT vs T plot for Q_5•2Cu at 1000 and 10000 Oe. Right: Magnetic field dependence of the magnetization for Q_5•2Cu at 1.85 K. Open circles are experimental data and lines are best fit results as discussed in the experimental section.

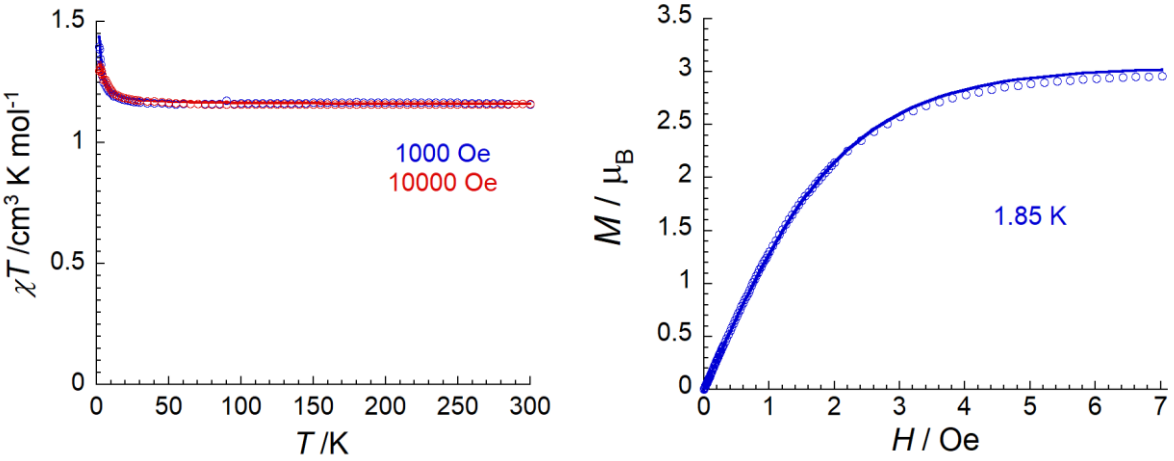

Figure S22: Left : Temperature dependence of the dc susceptibility, χ (defined as M/H per complex), shown as a χT vs T plot for Q_7•3Cu at 1000 and 10000 Oe. Right: Magnetic field dependence of the magnetization for Q_7•3Cu at 1.85 K. Open circles are experimental data and lines are best fit results as discussed in the experimental section.

6.6 SAM analysis

Table S2: Thickness of the self-assembled monolayers (SAM) on gold surface formed with Cu(II) loaded $AsgQ_n$ (n = 5, 9, 17) oligomers obtained by ellipsometry analysis. The thickness of the SAM obtained increases linearly with increasing foldamer length. This is only possible if the molecules are oriented perpendicular with respect to the surface of the substrate. If the molecules lie flat, then the thickness of the SAM would correspond to the diameter of the foldamer and remain constant with increasing foldamer length.

compounds	$AsgQ_5$•2Cu	$AsgQ_9$•4Cu	$AsgQ_{17}$•3Cu
Thickness (nm)	1.1 (±0.1)	1.9 (±0.2)	3.1 (±0.2)

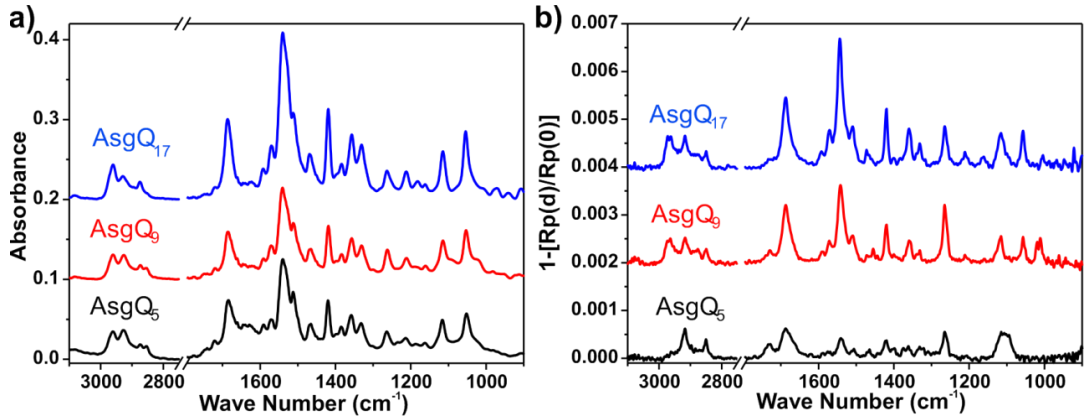

Figure S23: a) FTIR spectra of $AsgQ_n$ (n = 5, 9, 17) oligomers and b) The PM-IRRAS spectra of self-assembled monolayers (SAMs) on gold surface of $AsgQ_n$ (n = 5, 9, 17) oligomers. Comparison of the PM-IRRAS spectra with respective FTIR spectra indicates the formation of SAMs on gold surfaces of those oligomers. We note that there are no transitions are extinguished or appear when foldamers of different lengths are compared. From this, we can deduce that all the foldamer assemblies investigated possess similar orientation with respect to the gold substrate. Furthermore, if this orientation were parallel (i.e. foldamers lying flat), then the intensity of the PM-IRRAS signals would be the same for all monolayers. Instead, we observe that the signal increases with increasing foldamer length. This can only be possible if the foldamers are oriented perpendicular (i.e. standing vertical or with a constant tilt angle) with respect to the substrate.

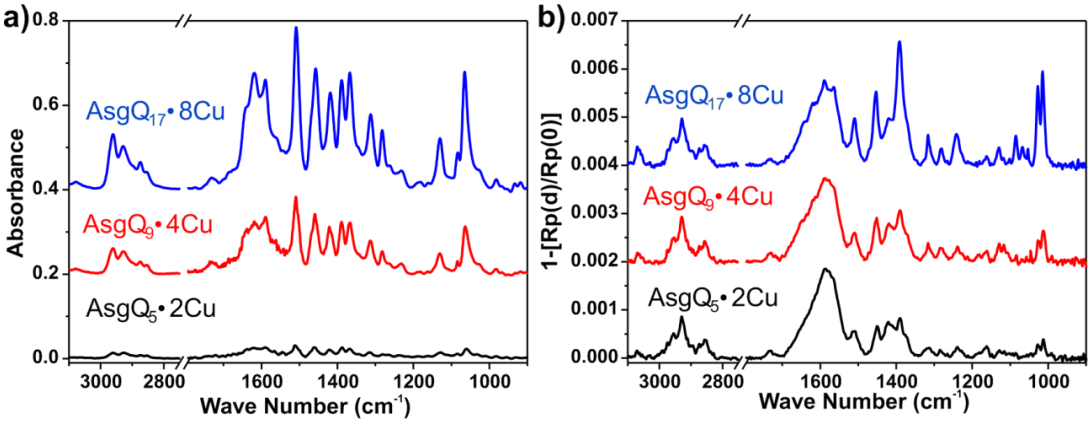

Figure S24: a) FTIR spectra of $AsgQ_n\bullet\frac{n-1}{2}Cu$ (n = 5, 9, 17) oligomers and b) The PM-IRRAS spectra of self-assembled monolayers (SAMs) on gold surface of $AsgQ_n\bullet\frac{n-1}{2}Cu$ (n = 5, 9, 17) oligomers. Comparison of the PM-IRRAS spectra with respective FTIR spectra indicates the formation of SAMs on gold surfaces of those oligomers. Differences in the intensities of some peaks between the PM-IRRAS spectra and respective FTIR spectra comes from the orientation of the SAMs on gold surfaces and the surface selection rule of PM-IRRAS.

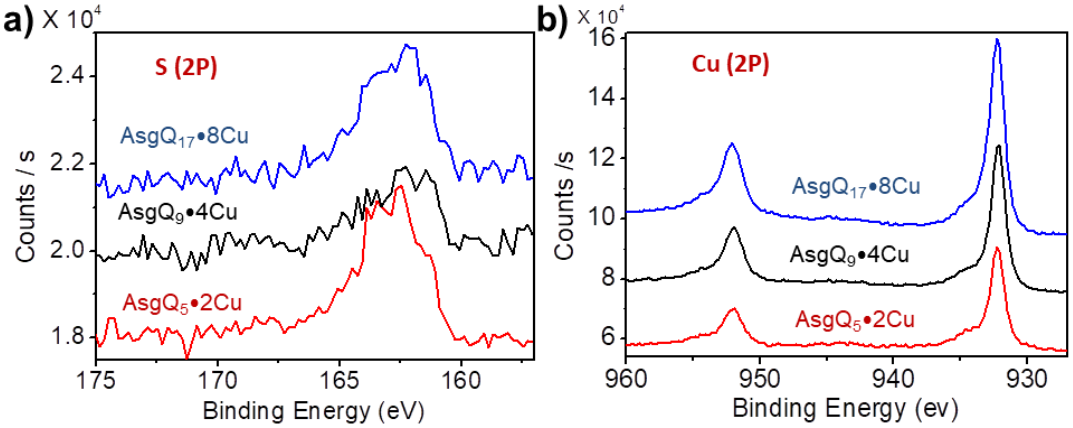

Figure S25: a) X-ray photoelectron spectroscopy of S(2p) region of SAMs on gold surfaces formed by Cu(II) loaded $AsgQ_n$ (n = 5, 9, 17) oligomers; and b) X-ray photoelectron spectroscopy of Cu(2p) region of SAMs on gold surfaces formed by Cu(II) loaded $AsgQ_n$ (n = 5, 9, 17) oligomers. The S(2p) and Cu(2p) signals indicate the elements S and Cu on the gold substrates from the copper loaded $AsgQ_n$ oligomers.

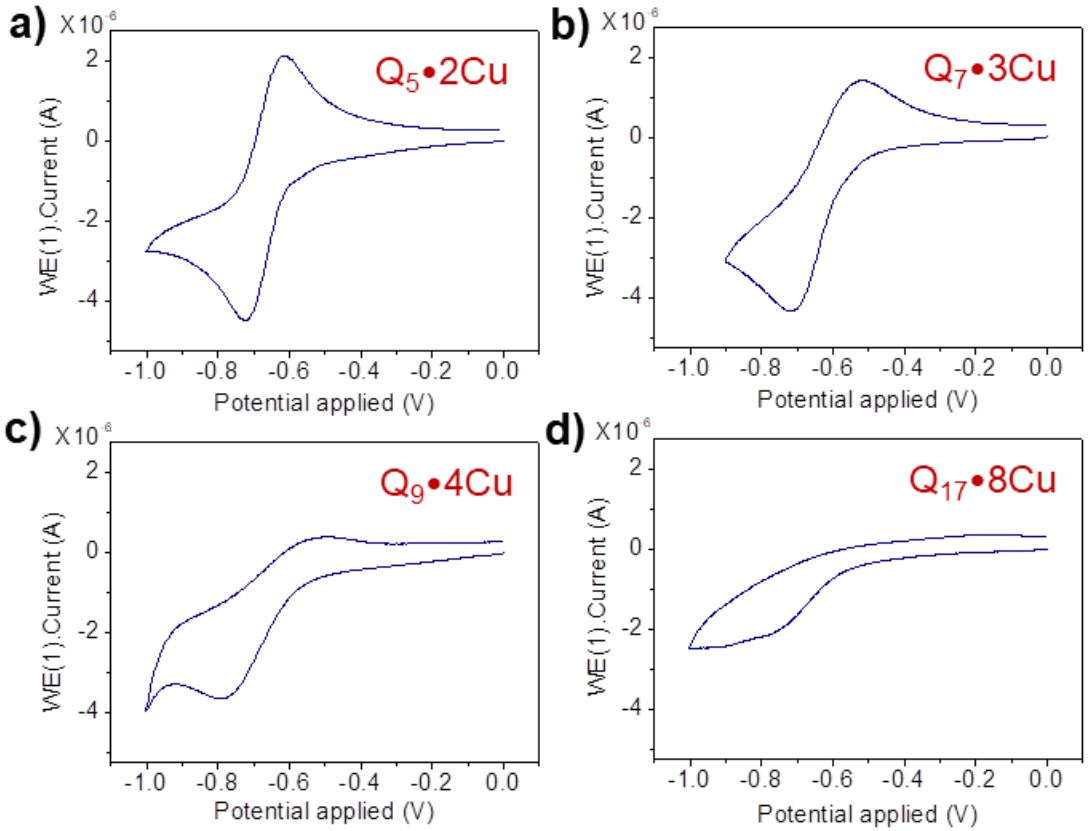

Figure S26: Cyclic voltamograms of a) Q_5•2Cu; b) Q_7•3Cu; c) Q_9•4Cu and d) Q_{17}•8Cu in solution. The concentrations of the Cu(II) loaded Q_n oligomers were 1 mM in DCM/CAN (vol/vol 1:3). The scan rate was 100 mV/s. Ag/AgCl was used as reference electrode. The reduction potential correlated well with the cyclic voltammograms of Cu(II)-loaded $AsgQ_n$ oligomers formed SAMs on gold surfaces. As shown in Table S2 and Figure S25, the area (and not Imax) of the voltammograms trends with the number of Cu(II) ions. In the case of the longer AsgQ17•8Cu complex, we can expect that some comproportionation exists between the redox-active sites, and that these will not undergo reduction at exactly the same potential nor at the same rate. This will of course result in broadening of the redox wave seen in the cyclic voltammetry. Assuming equal surface coverage, the number of electrons exchanged will depend on the number of adsorbed electroactive species in each assembly.

Table S3 : Integrated peak area and corresponding calculated surface density[a] obtained from cyclic

votammetry using the SAMs of gold electrodes obtained by Cu(II) loaded $AsgQ_n$ oligomers.

entry	$AsgQ_5$•2Cu	$AsgQ_9$•4Cu	$AsgQ_{17}$•8Cu
C_n (F/cm^2)	6.95×10^{-10}	9.55×10^{-10}	1.81×10^{-9}
Surface density (molecules/cm^2)[a]	2.09×10^{14}	1.44×10^{14}	1.36×10^{14}

[a]Calculated from geometrical area of electrode without taking into account surface roughness. Importantly, we note that the surface coverage is quite similar and independent of foldamer length

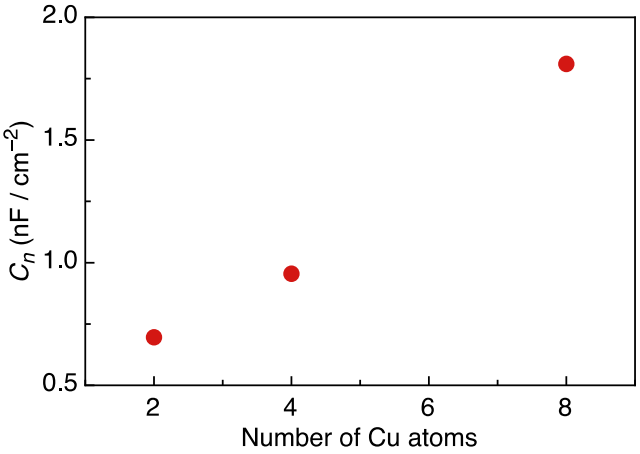

Figure S27: Graph of the C_n of the reductive wave for the Cu(II)-loaded $AsgQ_n$ SAMs vs. the number of Cu(II) ions bound in the oligomers. Cyclic voltammetry of monolayers on conductive substrates provides signals whose intensity is directly related to the number of charges exchanged between the electrode and the monolayer. The experimental results (Table S3) show that the number of charges exchanged (Cn) increases with increasing foldamer length. This would not be the case if the foldamers were lying flat, in which case the surface density of the redox-active sites would be constant. From this data, we may further calculate the surface density of the electro-active species (Table S3).

6.7 Conductive AFM

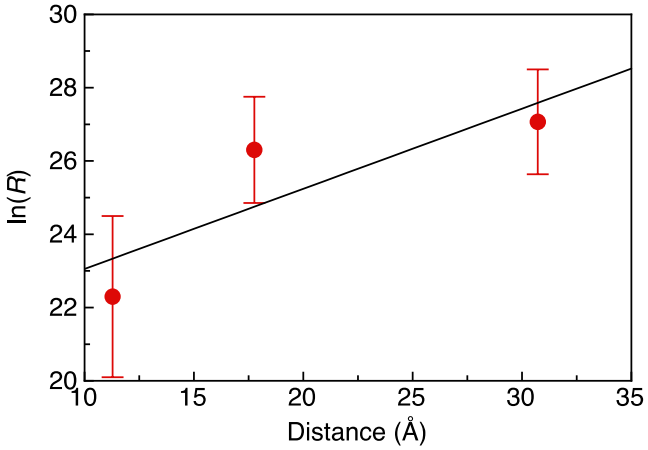

Figure S28: Semi-log plot of the vertical resistance of the Cu(II)-loaded $AsgQ_n$ SAMs as determined by c-AFM (applied tip force = 5.1 nN) vs. molecular length. The straight line is best fit with a slope of 0.22 ± 0.05 Å^{-1} (r = 0.85).

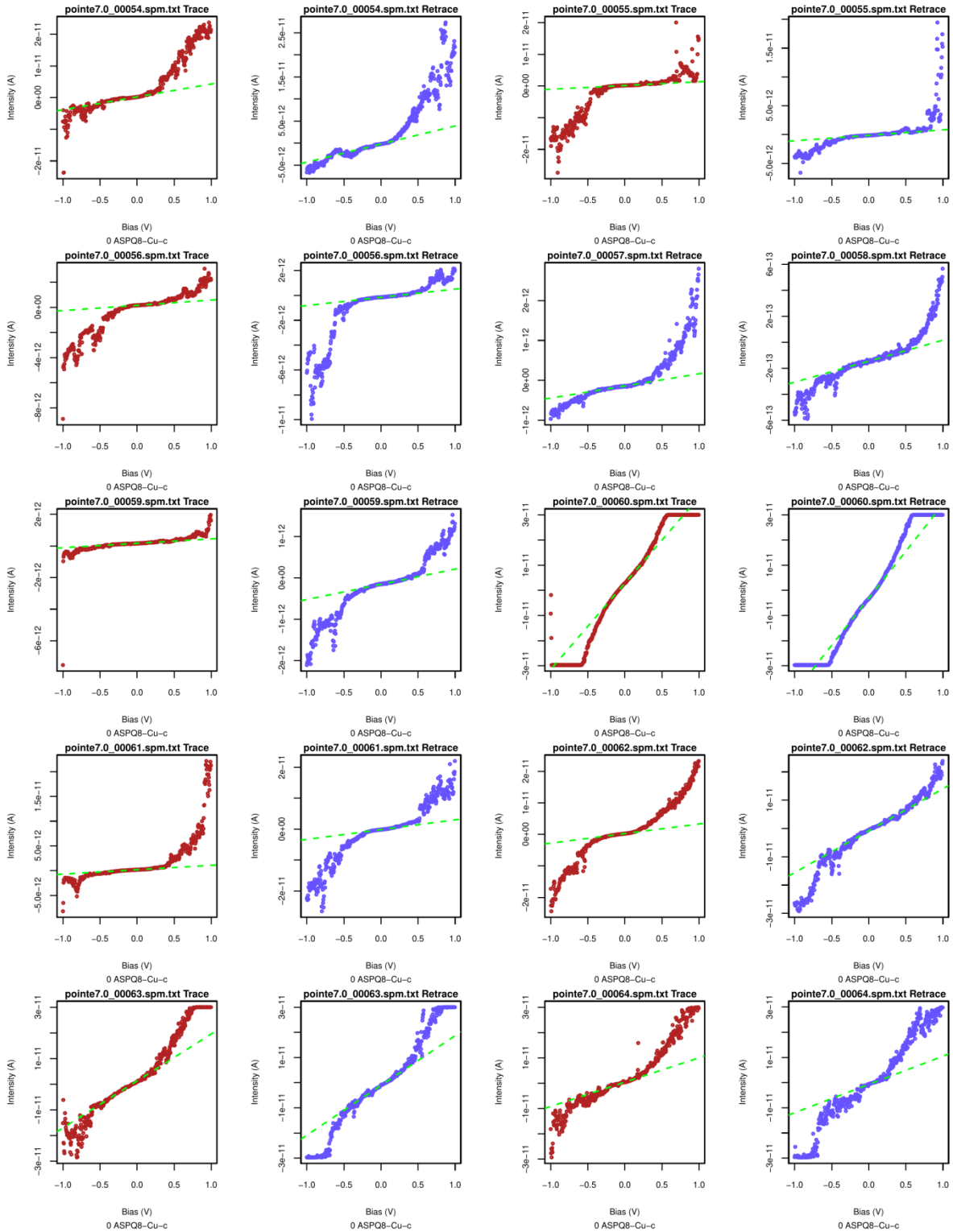

Figure S29: *I-V* curves acquired for SAMs of Cu(II)-loaded $AsgQ_n$ (n = 5, 9, 17) oligomers by c-AFM (applied tip force = 5.1 nN). Red and blue points represent data acquired by reversing the bias forwards and backwards. (1/5, to be continued)

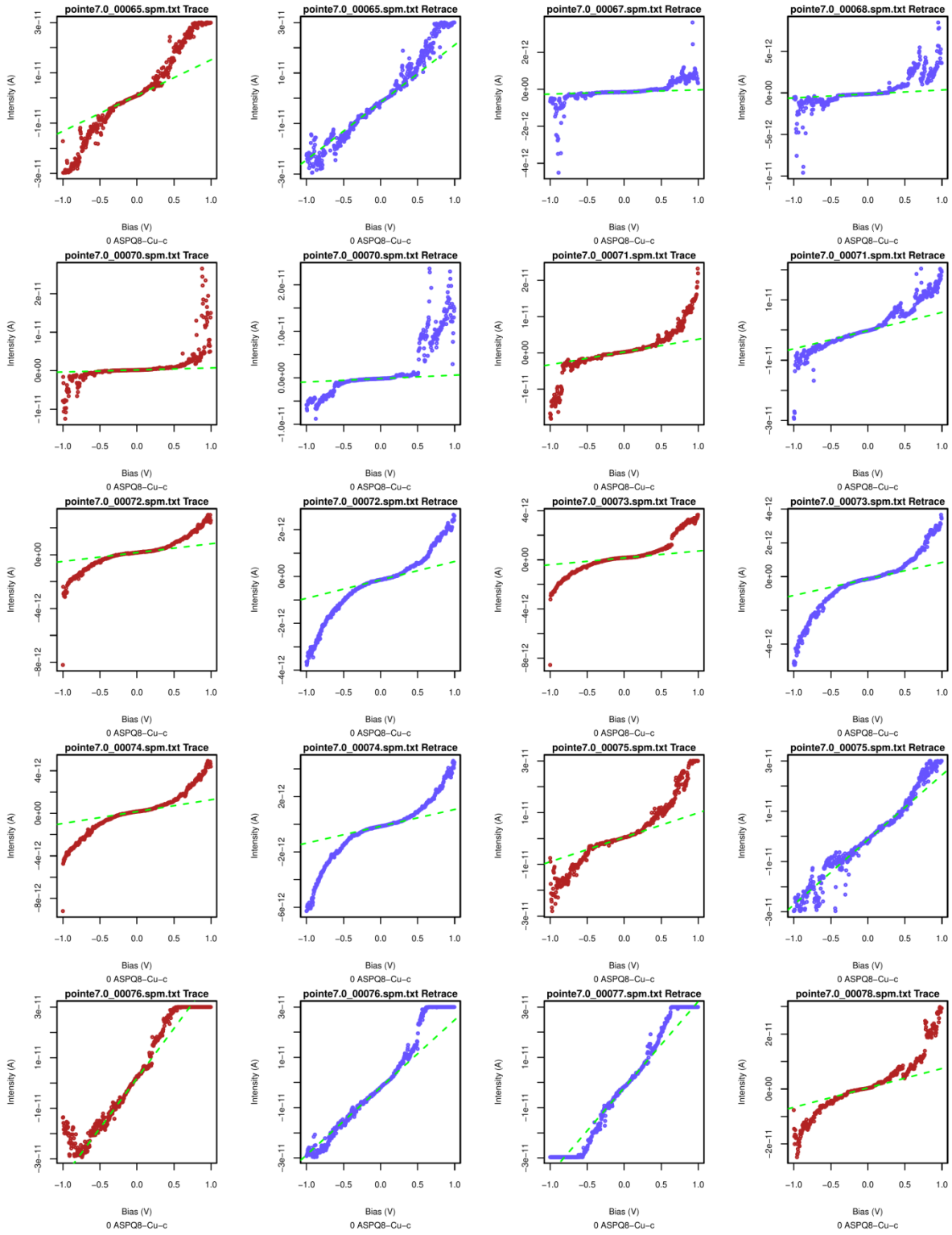

(Continuation of **Figure S29**, 2/5)

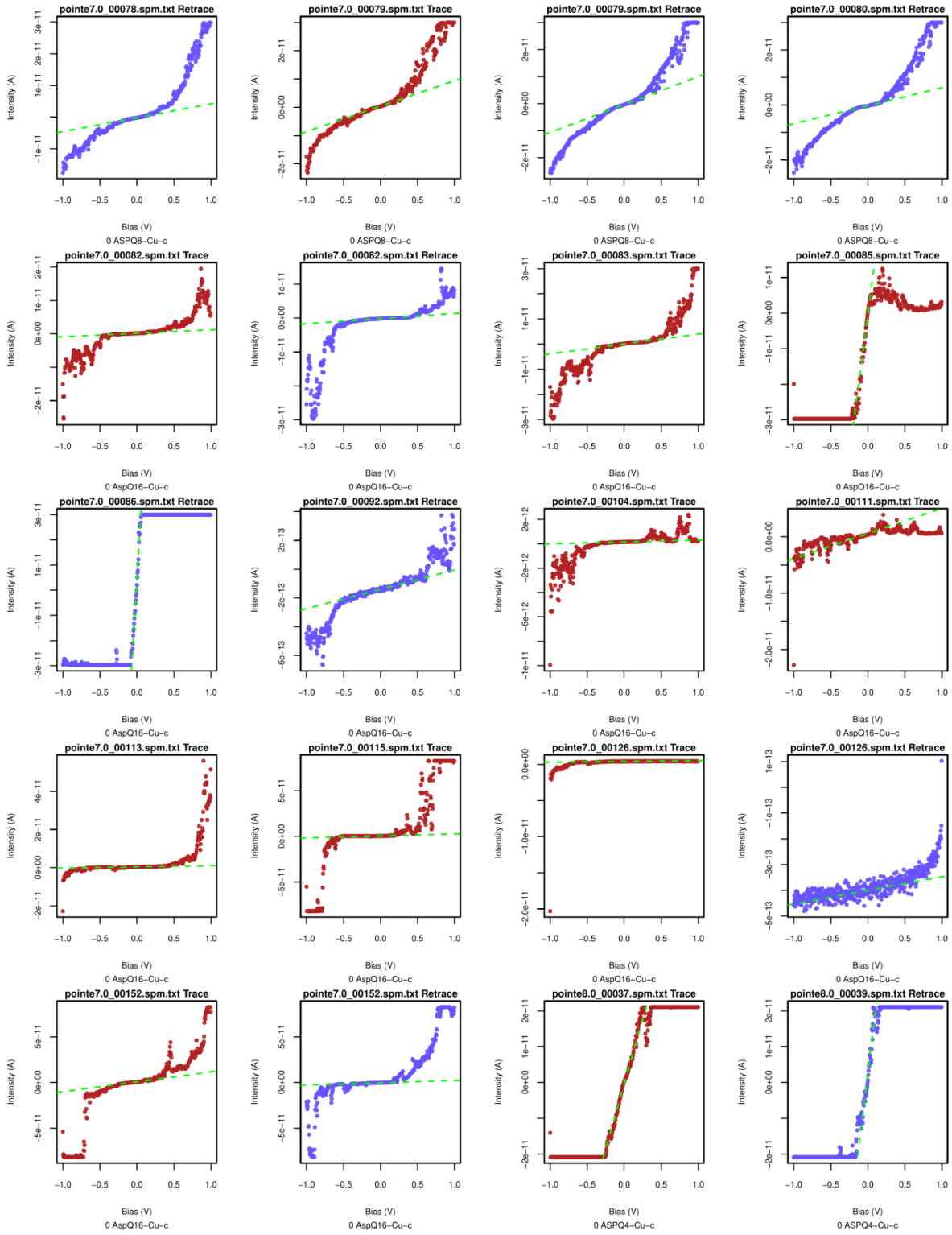

(Continuation of **Figure S29**, 3/5)

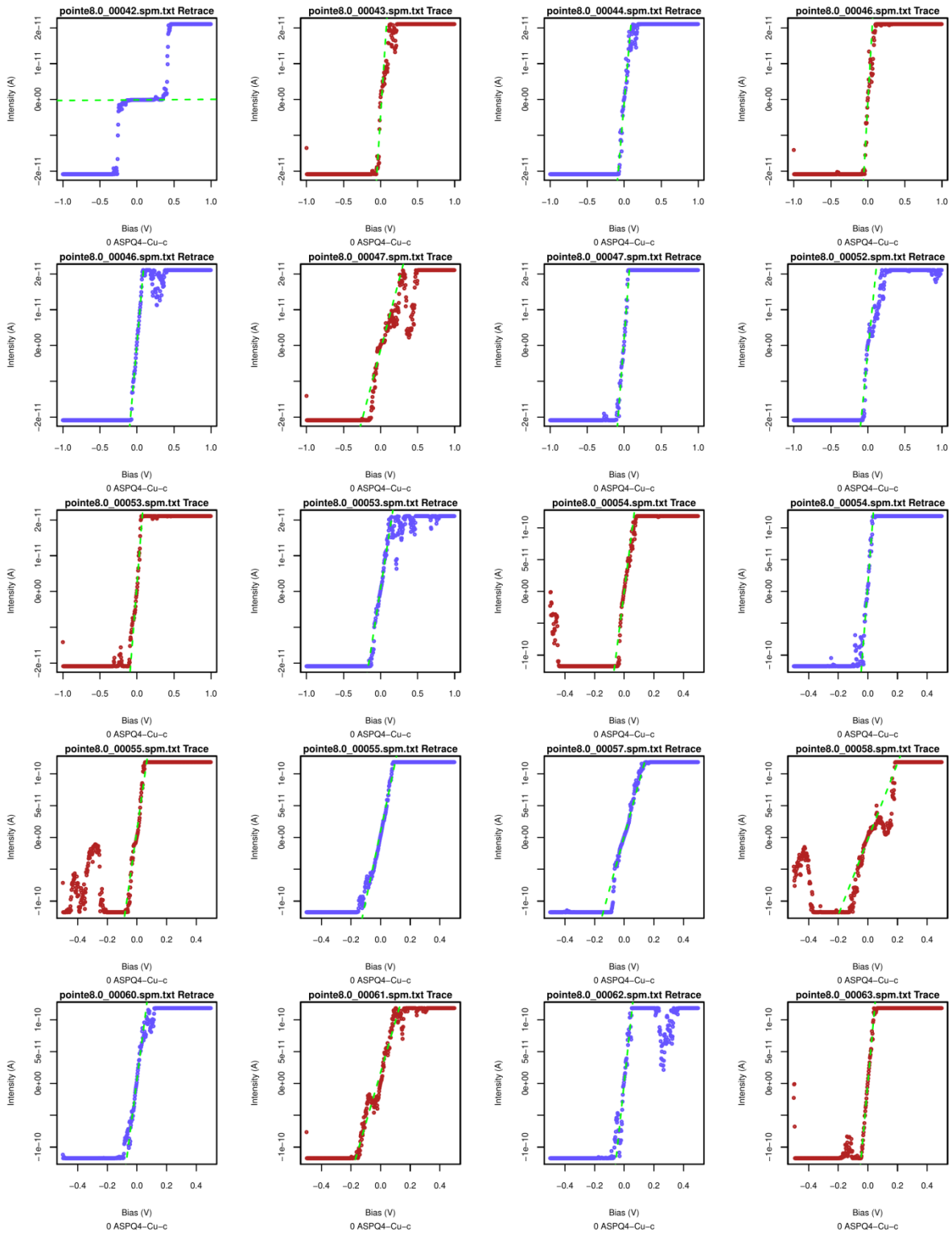

(Continuation of **Figure S29**, 4/5)

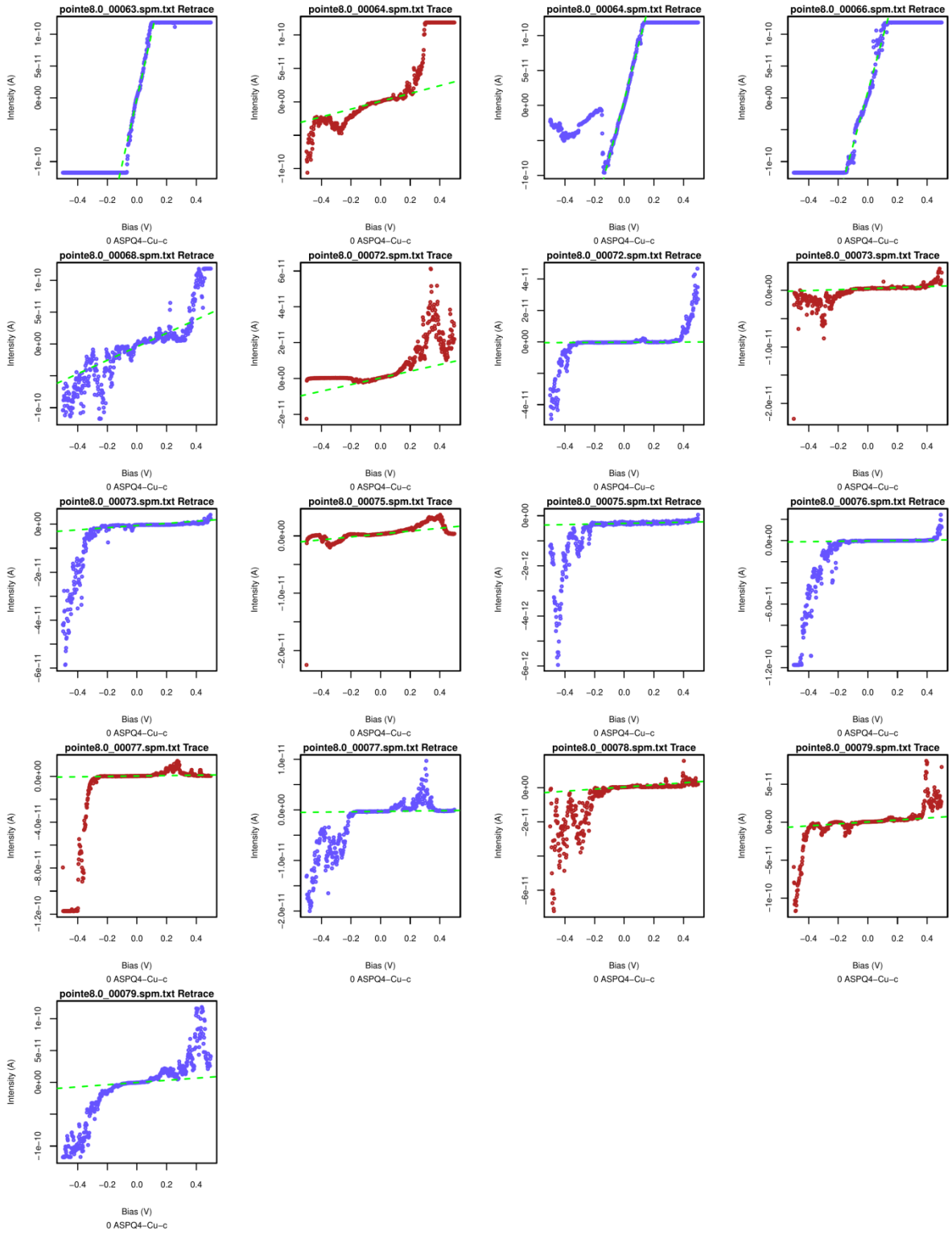

(Continuation of **Figure S29**, 5/5)

6.8 NMR and mass spectra of new compounds

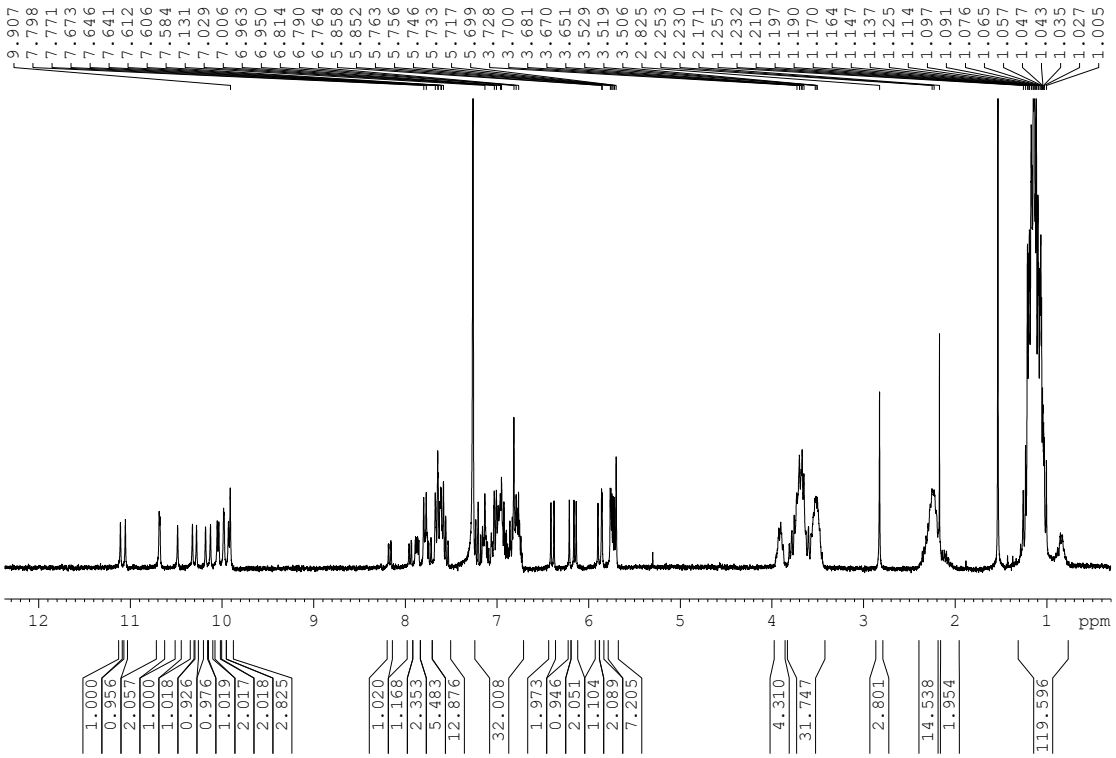

Figure S30: ^{1}H NMR of Q_{17} in $CDCl_3$ (300 MHz).

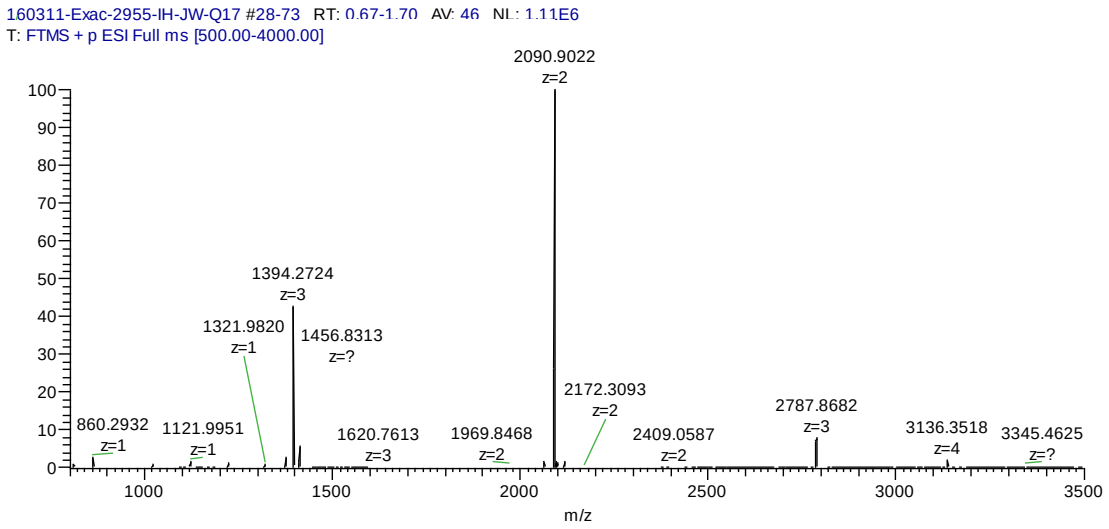

Figure S31: ESI+ HRMS of Q_{17}.

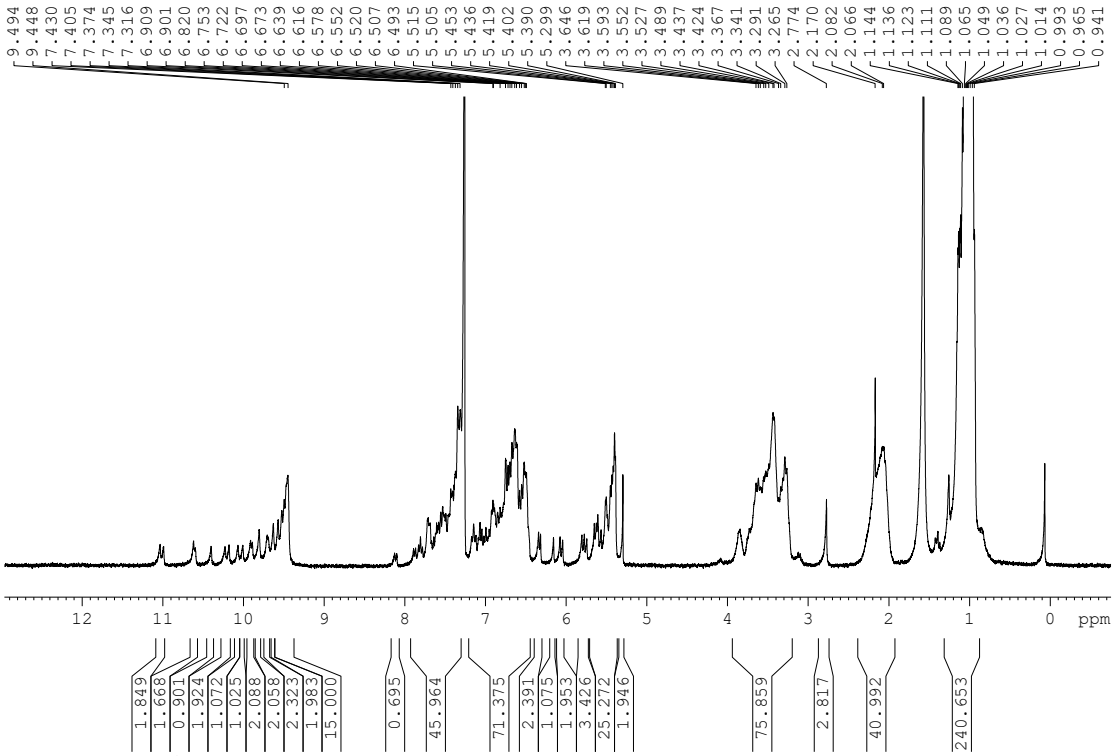

Figure S32: ^{1}H NMR of Q_{33} in $CDCl_3$ (300 MHz).

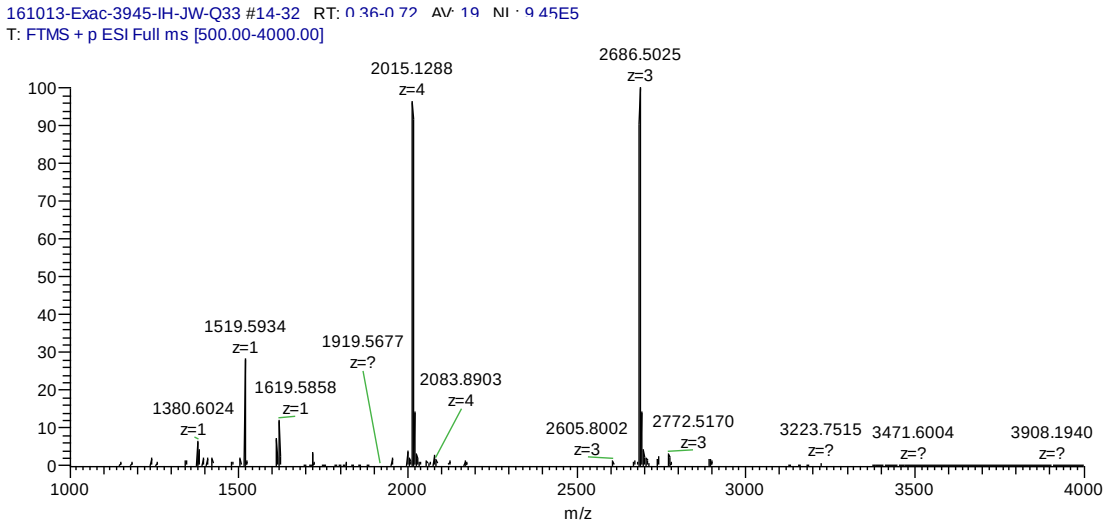

Figure S33: ESI+ HRMS of Q_{33}.

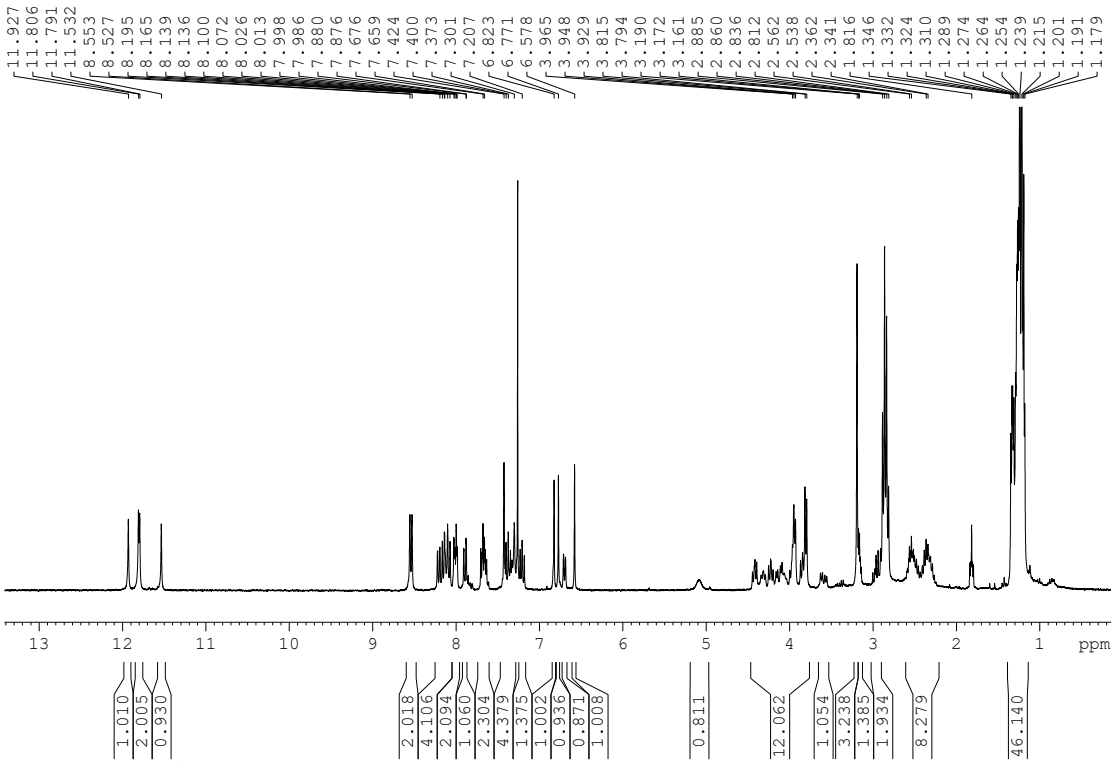

Figure S34: ^{1}H NMR of AsgQ$_5$ in CDCl$_3$ (300 MHz).

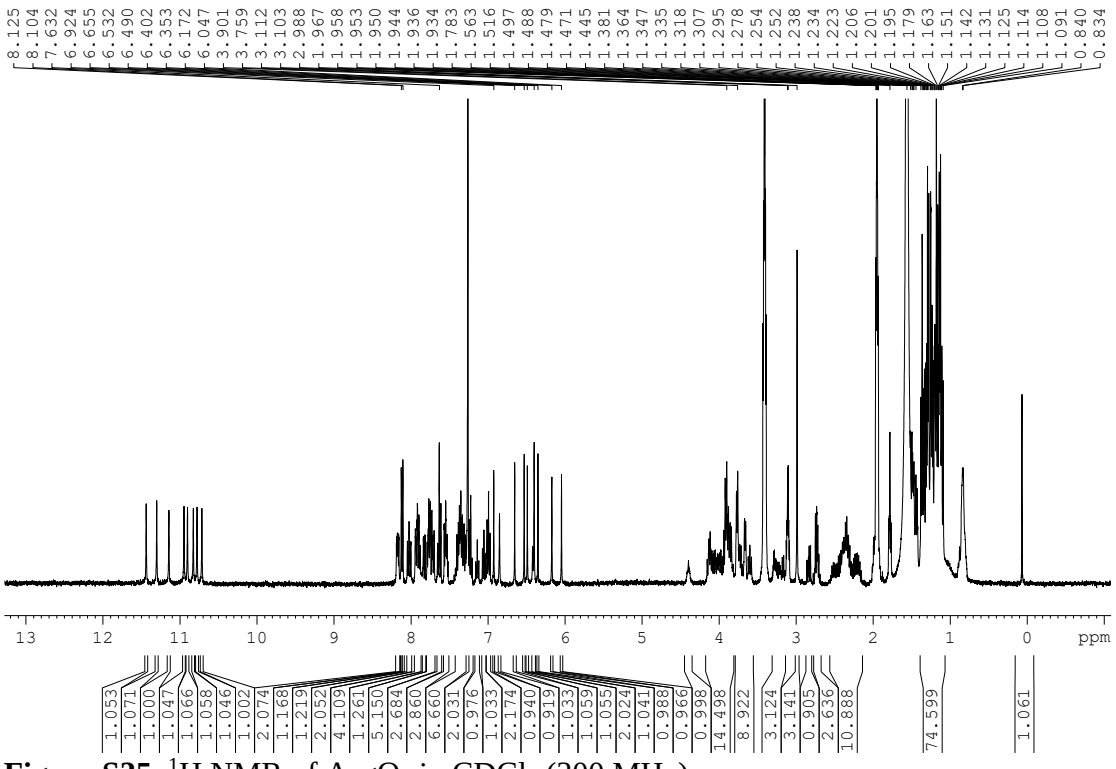

Figure S35: ^{1}H NMR of AsgQ$_9$ in CDCl$_3$ (300 MHz).

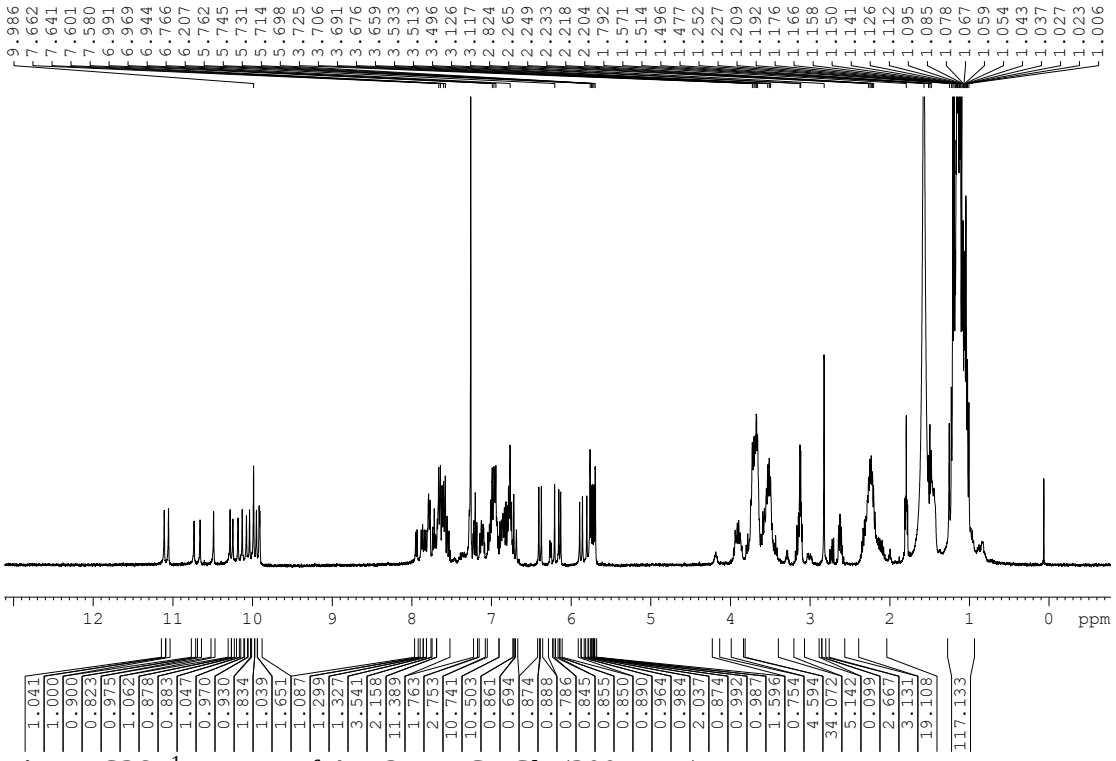

Figure S36: ^{1}H NMR of $AsgQ_{17}$ in $CDCl_3$ (300 MHz).

7. References:

[1] N. Delsuc, T. Kawanami, J. Lefeuvre, A. Shundo, H. Ihara, M. Takafuji, I. Huc, *ChemPhysChem* **2008**, *9*, 1882-1890.

[2] T. Qi, T. Deschrijver, I. Huc, *Nat. Protoc.* **2013**, *8*, 693.

[3] a) X. Li, T. Qi, K. Srinivas, S. Massip, V. Maurizot, I. Huc, *Org. Lett.* **2016**, *18*, 1044-1047; b) X. Li, N. Markandeya, G. Jonusauskas, N. D. McClenaghan, V. Maurizot, S. A. Denisov, I. Huc, *J. Am. Chem. Soc.* **2016**, *138*, 13568-13578.

[4] A. Méndez-Ardoy, N. Markandeya, X. Li, Y.-T. Tsai, G. Pecastaings, T. Buffeteau, V. Maurizot, L. Muccioli, F. Castet, I. Huc, D. M. Bassani, *Chem. Sci.* **2017**, *8*, 7251-7257.

[5] a) R. Singh, G. M. Whitesides, *J. Am. Chem. Soc.* **1990**, *112*, 1190-1197; b) L. Schotte, H. Ström, *Acta Chem. Scand.* **1956**, *10*, 687-688.

[6] a) M. A. Ramin, G. Le Bourdon, N. Daugey, B. Bennetau, L. Vellutini, T. Buffeteau, *Langmuir* **2011**, *27*, 6076-6084; b) T. Buffeteau, B. Desbat, J. M. Turlet, *Appl. Spectrosc.* **1991**, *45*, 380-389.

[7] T. Buffeteau, B. Desbat, D. Blaudez, J. M. Turlet, *Appl. Spectrosc.* **2000**, *54*, 1646-1650.

[8] D. J. Wold, C. D. Frisbie, *J. Am. Chem. Soc.* **2000**, *122*; 2970-2971.

[9] N. F. Chilton, R. P. Anderson, L. D. Turner, A. Soncini, K. S. Murray, *J. Comput. Chem.* **2003**, *34*, 1164-1175.

[10] CrystalClear-SM Expert 2.1 (*Rigaku* 2013) Software, Version 5.6.2.0, Tokyo, Japan.

[11] G. Sheldrick, *Acta Cryst.* **2015**, A*71*, 3-8.

[12] M. C. Burla, R. Caliandro, M. Camalli, B. Carrozzini, G. L. Cascarano, L. De Caro, C. Giacovazzo, G. Polidori, R. Spagna, *J. Appl. Crystallogr.* **2005**, *38*, 381-388.

[13] O. V. Dolomanov, L. J. Bourhis, R. J. Gildea, J. A. K. Howard, H. Puschmann, *J. Appl. Crystallogr.* **2009**, *42*, 339-341.

[14] G. Sheldrick, *Acta Cryst.* **2015**, C*71*, 3-8.

[15] A. Spek, *Acta Cryst.* **2015**, C*71*, 9-18.